Naval Research Laboratory
Washington, DC 20375-5320

NRL/MR/5320--93-7181

Comparison of RADARC High-Frequency Radar Performance Prediction Model and ROTHR Amchitka Data

BENJAMIN T. ROOT
JAMES M. HEADRICK

Advanced Radar Systems Branch
Radar Division

July 16, 1993

Approved for public release; distribution unlimited.

REPORT DOCUMENTATION PAGE

Form Approved
OMB No. 0704-0188

1. AGENCY USE ONLY (*Leave Blank*)	2. REPORT DATE	3. REPORT TYPE AND DATES COVERED
	July 16, 1993	

4. TITLE AND SUBTITLE

Comparison of RADARC High-Frequency Radar Performance Prediction Model and ROTHR Amchitka Data

5. FUNDING NUMBERS

PE - 204577N
WU - DN 291-215
TA - 148-NRL-VARI-002

6. AUTHOR(S)

Benjamin T. Root and James M. Headrick

7. PERFORMING ORGANIZATION NAME(S) AND ADDRESS(ES)

Naval Research Laboratory
Washington, DC 20375-5320

8. PERFORMING ORGANIZATION REPORT NUMBER

NRL/MR/5320--93-7181

9. SPONSORING/MONITORING AGENCY NAME(S) AND ADDRESS(ES)

Space and Naval Warfare Systems Command
Washington, DC 20363-5100

10. SPONSORING/MONITORING AGENCY REPORT NUMBER

11. SUPPLEMENTARY NOTES

12a. DISTRIBUTION/AVAILABILITY STATEMENT

Approved for public release; distribution unlimited.

12b. DISTRIBUTION CODE

13. ABSTRACT (*Maximum 200 words*)

Data collected with AN/TPS-71 radar has been used to validate the RADARC model. For the first ten days of January , April, and July, noon and midnight, the vertical ionograms, oblique backscatter soundings, radar ground backscatter amplitudes and noise levels have been compared with Model predictions. The differences between the Model and median ionospheric soundings are small enough to have negligible effect on predictions. The coverage predicted for oblique backscatter soundings agrees well with observed median data except for sporadic E effects which were under-estimated. Medians of observed ground backscatter agree fairly well with predictions. The actual noise that controlled radar performance was the most significant deviation from the model; all nighttime and January day noise was higher than that predicted; and this was due to "multiplicative" noise.

14. SUBJECT TERMS

Ionospheric Models
OTH RADAR
Skywave Transmission

15. NUMBER OF PAGES

62

16. PRICE CODE

17. SECURITY CLASSIFICATION OF REPORT	18. SECURITY CLASSIFICATION OF THIS PAGE	19. SECURITY CLASSIFICATION OF ABSTRACT	20. LIMITATION OF ABSTRACT
UNCLASSIFIED	UNCLASSIFIED	UNCLASSIFIED	UL

NSN 7540-01-280-5500

Standard Form 298 (Rev. 2-89)
Prescribed by ANSI Std 239-18
298-102

Contents

COMPARISON OF RADARC HIGH-FREQUENCY RADAR PERFORMANCE PREDICTION MODEL AND ROTHR AMCHITKA DATA

1. Introduction

RADARC is NRL's high-frequency radar performance prediction program.* It uses a model with both deterministic and statistical elements to solve the radar equation for the conditions that are expected to prevail in a particular location and time. This requires a correct understanding of both the radar system and the environment. We must know the various gains and losses in the system, which result from both hardware and signal processing. We must also predict the likely path of the radar beam through the ionosphere, the various path losses, the target reflectivities, and the environmental noise. Such radar performance modeling is useful not only for efficient operation of the system, but also in the design of such systems.

Many of the factors entering the model are statistical. For example, the ionosphere is described by a monthly median for each hour of the day. This description includes the number of electron density layers, the shape, height, thickness, and density of these layers, and resulting quantities such as the critical frequencies. In the case of sporadic E, we do not have a basically geometric model with statistically varying parameters, but use a wholly statistical description. Since the description is by monthly median, the actual ionosphere on any particular day may depart significantly from the prediction, and this can lead to considerable differences in the path of the radar beam, even to refraction from a completely different layer than predicted.

The environmental noise is also described by a monthly median for a given time of the day. Whether a radar is internally or externally noise limited is one of the important issues in radar performance. Not only is the noise model statistical, it is not appropriate for general application. For instance, we assume isotropic noise when in fact the noise can be direction-dependent. RADARC uses the CCIR noise curves that were first developed from an empirical database in the early 60's and have recently been revised [3,4].

It may be thought that we have better understanding and control of the radar system itself, but even here there are many unknowns. In particular the large size of a high-frequency radar (a kilometer or more in length) means that it is difficult to measure its true gain, and this gain is complicated by the environment in a way that does not occur for smaller radars. Even with a knowledge of the environment, we must resort to numerical software to estimate the gain, and these calculations are only approximate. The issue of gain can be important because with over-the-horizon radars it is often the lowest rays which reach distant targets, and the gain falls off rapidly as we graze the horizon. Furthermore, an HF radar is so large and complicated that it may be difficult to calibrate it with complete assurance, and we may underestimate or overestimate the various internal gains and losses. And it is more difficult to shield such a radar from changes in the external environment.

Manuscript approved May 13, 1993.

* It is the current version of the RADAR performance program described in NRL Memorandum Report 2226 [1]. The ionospheric model used is given in NRL Report 8321 [2].

One way of correcting and improving radar prediction programs such as RADARC is to test and validate them against new radar data. Recently, a new ROTHR (Relocatable Over-the-Horizon Radar) has been installed on Amchitka in the Aleutian Islands. A large quantity of radar data has been collected and sent to several laboratories, including NRL, for analysis. This data covers all hours of the day for about ten days in each of three months: January, April, and July of 1991. These three months give a sample of three different seasons. In this report we have processed data for each of the three months. In each month two different hours have been analyzed: 0 UT, which gives an example of the daytime (noon in Amchitka), and 12 UT, which gives an example of the nighttime (midnight in Amchitka).

- 00 UT (noon in Alaska) and 12 UT (midnight)
- January, April, and July, 1991
- First 10 days of month
- Azimuthal sector 0° to 10° (from boresight = 270° CWN)
- 500 - 1500 nm: mostly sea with many scattered islands
- 1500 - 2000 nm: half land

Table 1. ROTHR Amchitka data set analyzed in this report.

Note that we have simplified the analysis by selecting from an azimuthal sector extending from 0° to 10° with respect to boresight. (Boresight is at 270° clockwise from north.) This keeps the geography, and hence the surface reflectivity, approximately constant over azimuth at a given range. This azimuthal sector is shown shaded on the following map.

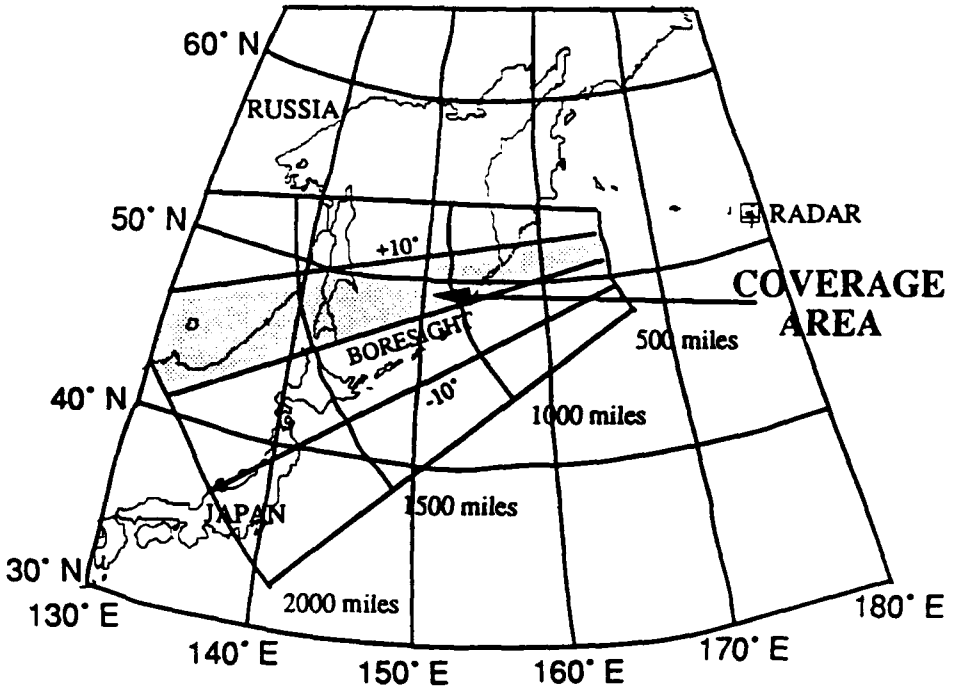

Figure 1. Azimuthal sector examined in this report

We have examined **three types of data.** The first consists of the **quasi-vertical ionograms** (QVIs), which give a description of the ionosphere overhead at the radar site. If we cannot accurately predict the local ionosphere, then we cannot hope to tackle the more complicated backscatter problem involving propagation effects as well as ionospheric gradients. So it is natural to first check how well the predicted and measured QVIs match. Then we consider the **widesweep backscatter ionograms** (WSBIs), which provide a synoptic view of backscattered power vs. frequency and range, but without doppler. Here, propagation effects are important, and we need to model correctly the gradients in the ionosphere over range. This is perhaps the ideal data type with which to test the RADARC model, because of its broad view of radar performance over range and frequency. We can detect patterns that might not be apparent with a narrow look at the backscatter at one operating frequency, even though the latter is far more sensitive and has doppler. We will compare the measured WSBIs with the RADARC predicted clutter-to-noise ratio map, as the two are closely related. However, one disadvantage of the WSBI is its lack of doppler, which may make it difficult to distinguish clutter from noise. Therefore, we finish our analysis with a detailed look at the actual range-doppler-amplitude data that the radar uses to find targets.

The **new environment** at Amchitka brings new problems. Of particular concern is the issue of **spread-doppler clutter**. The radar's propagation path crosses regions of the ionosphere near the equator containing irregularities in the electron density after sunset. These irregularities lead to the phenomenon of spread-doppler clutter: the range-folded equatorial Bragg reflections from land and sea near 0 Hz are spread out on the doppler axis and may mask targets. The problem is especially noticeable at night, because of reduced D-layer absorption. It leads to an effective increase in the noise floor above the atmospheric noise predicted by CCIR. Reliable radar performance requires that we correctly account for this problem. Also, the new environment may lead to variations in system performance from what is expected from previous locations. In particular, the gain may be different, but so may other parts of the system.

Finally, a program as complicated as RADARC may have had unnoticed defects or deficiencies that have gone uncorrected. It has never been validated against a database as extensive as what we have recently collected in Amchitka. Analyzing this data should lead to a better understanding of the radar, not only for this particular environment, but for all environments.

The overall objective of the analysis in this report is summarized in the table below.

• Compare ROTHR data from Amchitka with RADARC high-frequency radar performance prediction model.
• Compare measured "clutter" and "noise" (defined on p.13) with predicted clutter and noise.
• Make corrections and improvements to model as needed.

Table 2. Objective of the analysis in this report

2. Comparison of RADARC Prediction of Quasi-Vertical Ionograms (QVIs) with ROTHR Data

2a. Description of Analysis

The QVIs show time delay vs. frequency for a vertically transmitted pulse. The "quasi" in quasi-vertical comes from the small separation (~20 miles) between transmitter and receiver. The vertical ionogram is one of the oldest methods for probing the ionosphere. At a frequency below the critical frequency of a given ionospheric layer, the pulse is reflected before reaching the height of maximum ionization, which results in some finite delay for the received pulse. As the transmitted frequency approaches the critical frequency, the time delay increases, becoming theoretically infinite at the critical frequency. Above the critical frequency, the pulse penetrates the layer and continues to the next layer, where this process is repeated, or else it escapes into space. A trace of time delay vs. frequency results. Actually, there are two closely spaced traces, one for the ordinary ray and another for the extraordinary ray. At frequencies far below critical, the two curves overlap. Near the critical frequency, both curves become nearly vertical, with about 0.5 to 0.8 MHz between them.

This method of probing the ionosphere measures integrated electron density along the pulse path. To some extent, the actual electron density distribution can be inferred, especially if an ionospheric model with adjustable parameters is assumed (such as parabolic layers). In general, though, it is not possible to probe a given layer above the height of maximum ionization, and the distribution below this height cannot be read directly but must be deduced by a numerically laborious procedure.

The ionospheric model in RADARC is the same as that in IONCAP, which in turn traces its database back to the late 1950s when a worldwide survey of the ionosphere was undertaken as part of the IGY (International Geophysical Year). Samples of the ionosphere were taken during solar maximum and minimum activity, and modeled between these years by interpolation. The ionograms in this database were "scaled" (measured) in the following way. The critical frequencies of the various layers were identified by the characteristic vertical slope of the traces. The "height" of the layer was simply taken as the first minimum of the trace below the critical frequency, which actually corresponds to the bottom of the layer. Unfortunately, the frequency of this local minimum was not always recorded, only the height (time delay) itself. Sometimes there is no clear separation between layers (especially with the F1 layer), and the various possible layers are not always present. Also, obscuring sporadic-E can complicate the problem.

RADARC predicts a vertical ionogram for each of the control points specified in the model. The separation between ROTHR transmitter and receiver is sufficiently small that we can directly use the RADARC ionogram at the transmitter for comparison with the ROTHR QVI. A QVI is taken about every 12.5 minutes, which gives us about 45 QVIs per hour per month (for the first 10 days). There is considerable variability in the measured QVIs, especially from day to day, and some kind of average must be performed. We take a **median QVI** by the method described in the next section.

2b. Description of Software

We have about 45 QVIs per hour per month (first 10 days), which must somehow be reduced to one representative QVI for comparison with the RADARC prediction. Each QVI has about 230 frequency cells vs. 500 time delays. In principle, there is an amplitude in each of these frequency-delay cells, and the amplitude is quantized in 8 steps from noise to some clipping level.

We will not be concerned with absolute power levels, but only with finding a representative curve of time delay vs. frequency. So we begin by outlining such a trace on each individual QVI. In principle, such a procedure requires pattern recognition and artificial intelligence, but for the moment we shall be content with the following simple algorithm. At each frequency on the QVI, and starting at 50 km of time delay to avoid ground reflection, we scan upwards in time delay for the maximum in power. This is taken as the height of the first echo at that particular frequency. We record the time delay (or slant height) of that cell. When we have finished with all frequencies, we have a trace of time delay vs. frequency for one individual QVI. We repeat this procedure for all 45 or so QVIs of the month at the selected hour. We then take a median over all the resulting traces by finding the median height at each frequency. This finally gives us the one median ionogram which we compare with RADARC. An example of such a median ionogram is Figure 3.1 in Appendix A. These figures are discussed in detail in the next section. The algorithm is summarized in the following box.

- Step1: On each QVI, at each frequency, starting at 50 km and scanning upwards in time delay, find cell with maximum power.
- Step 2: Record slant height of this cell at each frequency.
- Step 3: Repeat with all QVIs (about 45) for the selected hour and month.
- Step 4: Take median over the resulting traces by finding median height at each frequency.

Table 3. Algorithm to extract median quasi-vertical ionogram

It should be noted that near the critical frequency, we will tend to pick up the extraordinary rather than ordinary trace, since the former extends somewhat higher in frequency. Fortunately, the ionograms predicted by RADARC specify the critical frequency of the extraordinary ray.

2c. Discussion

Table 4 summarizes our analysis of the median quasi-vertical ionograms presented in the figures of Appendix A. We have compared both the critical frequencies and the layer heights of the RADARC model with the ROTHR data. The critical frequency is defined as the frequency where the extraordinary ray becomes vertical. The layer height is defined as the bottom of the "valley" for the corresponding layer, assuming that such a local minimum is apparent. This is in accordance with how the database used in RADARC was originally "scaled," as discussed in Section 2a.

Critical Frequencies and Layer Heights

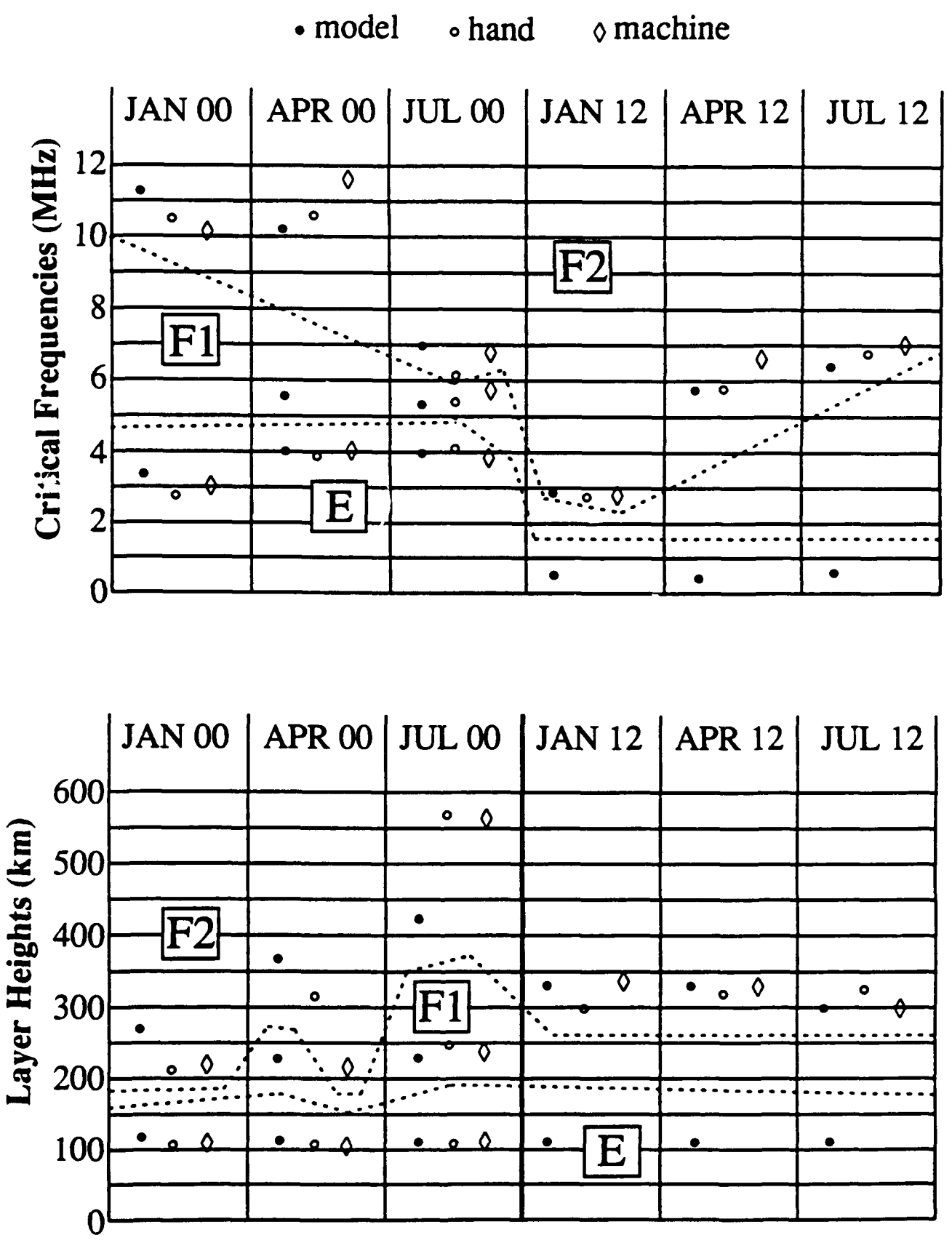

Table 4. Critical frequencies and layer heights of quasi-vertical ionograms

If a local minimum is not apparent, we choose the minimum height where the layer in question seems to start. This is especially relevant for the F1 layer, which often has a monotonic increase of height vs. frequency on the ionogram.

Our analysis of the data is twofold: on the one hand we read off the critical frequencies and layer heights from the median estimates generated by computer, as described in Section 2b; but on the other hand, we check this by examining all the individual ionograms by eye and forming an estimate based on patterns that are apparent to us from this visual inspection. The former method is called "**machine**" (open diamonds) in the table, and the latter method is called "**hand**" (open circles). Finally, we present the RADARC predictions (called "**model**") as black dots. The dashed lines identify the ionospheric layers (E, F1, or F2).

The computer-generated medians ionograms are shown in **Appendix A.** On these figures, the ROTHR median ionogram is represented by black dots, and the RADARC prediction by little plus signs. The month and hour are shown at the top of the plot. A numerical table of the RADARC prediction is shown in the upper right of the plot. We see the critical frequencies (FC), critical heights (HC), and semi-thicknesses (YM) for the E, F1, and F2 layers. This model assumes parabolic layers in all cases, so that HC is the height of maximum ionization and YM is the semi-thickness of the parabolic profile of electron density. It should be stressed that HC is *not* the layer height presented in Table 4. The latter corresponds to the bottom of the layer rather than to the middle of the layer, where the electron density reaches maximum. Finally, the last line the RADARC numerical table, marked by ES in the left column, describes the sporadic-E statistical estimate.

Traces were sketched by hand showing what the ionosphere was like on individual days, and these are shown in the inset on the figures of Appendix A. A single representative ionogram was chosen for each day, a piece of translucent paper was overlaid, and the ordinary ray was traced with pencil. The collection of these traces is presented superimposed in the inset. The number labeling each curve is the day of the month.

April day (hour 00 UT, Figure 3.3) was a **special case.** The individual ionograms showed such variability from day to day that it seemed that all seasons were occurring on some day or another within the month. (There was fortunately much less variability within a day, as one would expect.) The variability is quite apparent in the inset just described, and this explains why the computer-generated median performs poorly, and why we have poor agreement with the model. With such variability, it is doubtful whether any median model is meaningful as a description of the ionosphere.

For other months and hours, the comparison is generally satisfactory. (Remember that the ROTHR data is based on the first ten days of the month. One might reasonably question whether this provides an adequate statistical sample for the month as a whole.) The estimate of the critical frequencies tends to be better than estimates for the layer heights. This is expected, if we remember how the RADARC ionospheric database was originally constructed (see Section 2a). The critical frequencies are relatively unambiguous and easy to read on the ionograms. Furthermore, they are the most important parameter in predicting radar performance, as the radar tries to operate just below the critical frequency. Therefore, the RADARC database is "geared" towards the best possible estimate of critical frequencies. The layer heights, on the other hand, are often more ambiguous to identify on the ionograms, for the reasons given, and this is complicated by the fact that the original IGY analysis did not record the frequencies of the layer heights.

Our analysis of the quasi-vertical ionograms is summarized by the remarks in the table below.

- In general, first 10 days of month compare fairly well with model.
- April days deviate the most and are the most variable.
- Simple median algorithm gives fair results and could be improved.

Critical Frequencies:

- Model January & July midday F2 critical frequencies are high
- Good April agreement (of F2 criticals)
- Note that RADARC model includes fxF2 at high frequency end.
- E critical frequencies a bit high in January.
- F1 was observed in April less than half the time - a significant disagreement with model
- Model midnight F2 critical frequencies compare with hand analysis (after adding 0.7 MHz to foF2 to estimate fxF2).

Layer Heights:

- Daytime h'F2 observed ~50 km low in January and April, but ~150 km high in July.
- Daytime F1 and E layers show fair agreement.
- Night shows good agreement.

Table 5. Summary of analysis of quasi-vertical ionograms

3. Comparison of RADARC Prediction of Widesweep Backscatter Ionograms (WSBIs) with ROTHR Data

3a. Description of Analysis

The WSBIs show backscattered power over all ranges and frequencies, but without doppler. Of course, the transmitted power is much weaker than for the range-doppler data used to find targets. The WSBI provides an overall view of propagation conditions and helps in selecting the optimum operating frequency. It closely resembles the clutter-to-noise map predicted by RADARC and is therefore the ideal data for comparison with the RADARC model. The lack of doppler, however, can sometimes make it difficult to distinguish clutter form noise, or one type of noise from another.

About 45 WSBIs per hour per month reside in the database (the same as for the QVIs). There are two types of ROTHR WSBI data: one is clipped in amplitude above a certain threshold and the other is clipped below another threshold. The first type is used to avoid regions of weak backscattered power, and the second to scan the clutter environment and correlate with ionospheric models in the radar's computer system. We use the second type of data, since we are trying to correlate with RADARC's ionospheric model. The clipping floor for this data can be up to 64 dB below the peak amplitude.

The synoptic nature of the WSBI (the fact that it covers all ranges and frequencies) makes it easier to detect patterns in the discrepancy between the RADARC model and the radar performance. For instance, we can tell if there is a consistent bias in the leading edge of some propagation mode, or if the model and the data even agree on the modes of propagation. We can distinguish between sporadic E and normal layer propagation or between propagation from different layers with far greater ease than if we only have power vs. range at one frequency. Just by comparing the outlines of the clutter regions in the WSBIs and the RADARC CNR maps, we can obtain a good first order test of the RADARC model. If there is a large discrepancy in the outlines, we must resolve the major errors before be worry about fine-tuning the actual power levels. The present analysis will in fact concentrate on a qualitative or semi-quantitative comparison of the shape and location of the clutter in range-frequency space.

As with the QVI data, we reduce the 45 WSBI to one representative median ionogram for the hour and month for comparison with the clutter-to-noise map predicted by RADARC for that hour and month. The algorithm for performing this reduction is described in the next section.

3b. Description of Software

Each WSBI consists of about 230 frequency cells and 250 time delay (range) cells. The power is quantized into a 128-level scale of 1/2 dB steps extending down from the peak recorded amplitude. The reduction of the 45 WSBIs to one median WSBI is simpler than for the QVIs. There is no attempt at any kind of "pattern recognition" such as the simple algorithm to pick out the dominant trace in the QVI. Instead each range-frequency cell is averaged separately. That is, in each of the range-frequency cells, the algorithm determines the median power over all 45 ionograms for the selected hour and month. Due to the great number of range-frequency cells, some smoothing of the individual ionograms is done before the median is taken. The ionogram is partitioned into little boxes containing 3 frequency cells x 5 range cells, and a simple numerical average of these 15 cells is taken and recorded as one smoothed cell. The median is then taken from the 45 smoothed ionograms as just described. The algorithm for extracting the median WSBI is summarized in the following table.

- Step1: Each individual ionogram has 230 frequency cells x 250 range cells. These are first smoothed by taking the average power in a 3 by 5 window. The result is ~45 smoothed ionograms for each hour and month.
- Step 2: In each range-frequency cell of the smoothed ionograms, take the median power over all ionograms for the selected hour and month.

Table 6. Algorithm to extract median widesweep backscatter ionogram

3c. Discussion

The comparison between the ROTHR median widesweep-backscatter ionograms and the RADARC predicted clutter-to-noise ratio (CNR) maps is shown in the figures of Appendix B. The median WSBI is shown on the bottom left, and the CNR map on the bottom right. On the top are two small plots whose significance will be discussed shortly. On both the WSBI and the CNR map, a greyscale was simulated by altering the size of the little squares. The size (edge) of the square is proportional to dB below peak clutter power. (Perhaps the area of the square should have been made proportional to power for a more realistic visual effect.) As we have said, we cannot expect to correlate exact powers between model and data, but only general patterns. Nevertheless, it is a sufficiently difficult task to predict the general patterns of backscattered power, and good qualitative agreement with the data would be encouraging in itself.

It should be remembered that the "noise" levels in the WSBI and in the CNR map are not necessarily the same. The former is based on the ROTHR spectrum monitor measurement during the time the data was collected, and the latter is based on the CCIR prediction. One of our tasks is

to find discrepancies in these noise levels, especially as relates to the spread-doppler clutter phenomenon.

The small subplots at the top of the figures are an attempt to emulate the selection of operating frequency by the radar operator. A computer algorithm examines the corresponding plot below. At each range, it searches across frequency for the maximum power level, which should usually be near the leading edge. Since the data is quantized, there may be a number of equal maximum power cells. In this case, the one with the highest frequency is chosen. The power and frequency of this cell are recorded at each range. The power vs. range is shown as the solid curve, and the frequency vs. range as the dashed curve. This algorithm is still in the initial stages of development, and the results presented in the small subplots are for illustration only. It would be inadvisable to draw conclusions from them.

The comparison is necessarily qualitative and therefore subjective. The following table presents our opinion, and the corresponding figures can be consulted by the reader. As we have repeatedly emphasized, we do not expect precise agreement between the power levels, but we do hope for a good similarity in the shapes and patterns of the backscattered power. Considering how complex the ionosphere and propagation are, and how difficult it is to predict them, a good shape correlation should indicate a reasonably good model.

The major error in the model is in predicted Es coverage, and it errs in having both more and less than the measurements at different times.

	DAY (00 UT)	NIGHT (12 UT)
JAN	Good correlation for skip zone defined by F region	Good correlation for skip zone defined by F region More Es than predicted
APR	Good correlation for 1-hop skip zone Data does not show 1 hop - 2 hop division	Good skip zone correlation
JUL	Data has more Es than model <1200 nm: good skip zone correlation. Data does not show F region returns	Good F region skip zone correlation Model shows more Es than observed

Table 7. Comparison between model and data for widesweep-backscatter ionograms

4. Comparison of RADARC Prediction of Clutter and Noise with ROTHR Data

4a. Description of Analysis

In this analysis, we compare the radar performance predicted by the RADARC model with the actual performance of the ROTHR system in Amchitka during 1991. As indicated in the Introduction, we examine the radar data at **0 UT** (noon local time) and **12 UT** (midnight local time) for the **first 10 days of January, April, and July**. The radar data consists of received power for each range-doppler cell. The range and azimuthal resolution is relatively good, but we cannot discriminate in elevation. Our analysis consists primarily of comparing the "clutter" from land and ocean and the "noise" from the environment with that predicted by RADARC. (Both these terms are defined below.) By separating out the absolute powers of clutter and noise, we understand better what is happening than if we just look at the ratio of the two (as one usually does). The present analysis will emphasize this separation of clutter and noise.

We further narrow the data by selecting from an **azimuthal sector** extending from 0° to 10° with respect to boresight. (Boresight is at 270° clockwise from north.) This keeps the geography, and hence the surface reflectivity, approximately constant at a given range. Since the present version of RADARC assumes an average sea surface everywhere, we expect the actual reflectivity sometimes to be a significant source of error in the prediction. By examining a narrow sector, we simplify the analysis of a problem that has many sources of error, reflectivity being only one of them. The sector chosen is the one where the radar was most frequently tasked during the time of the data collection. It can be divided into two ranges intervals: one extending from 500 to 1500 nautical miles from the radar consisting mostly of sea with many scattered islands, and another extending from 1500 nm to 2000 nm consisting half of land and half of sea. See Figure 1.

The **clutter** is here defined to be the maximum power in a small window (+/- 2.0 Hz) around 0 Hz at each range. For the relatively large aircraft waveform repetition rates (WRF) selected in this analysis, the two Bragg peaks are generally not differentiated in the log-amplitude data, and so "clutter" is simply a measure of the backscattered power from sea or land against which a slow target must compete.

There are various possible definitions of **noise**. In the RADARC program, noise is selected to be the maximum of either the ROTHR system noise curves or the galactic and atmospheric noise* from the widely used CCIR prediction tables. In the ROTHR log amp data, noise is taken (at a particular range) as the average (in dB) of the clutter at + and - WRF/4 (in a doppler spectrum where 0 Hz is at the center). If there is no spread-doppler clutter, so that there is a flat noise floor outside of the clutter, then the two definitions of noise should agree closely (at least if the WRF is chosen so that the land and sea clutter is concentrated around 0 Hz). If there is spread-doppler that extends to +/- WRF/4, then this definition of "noise" will be higher than for RADARC. The points at which the noise is measured are taken to be representative points on the doppler axis, at the centers of the unambiguous positive and negative doppler extent. See Figures 2.1 and 2.2 for examples of radar data both with and without spread-doppler clutter.

---

* RADARC has a spread-doppler clutter model, but this has not yet been range-folded to ambiguous ranges such as Amchitka. Our comparison will indicate the presence of spread-doppler clutter by a large discrepancy between CCIR and measured noise.

RADARC predicts (among other things) the **clutter-to-noise ratio** (CNR). The clutter power is found by adding this ratio to the CCIR noise. The CNR radar equation modeled by RADARC is as follows.

$$\begin{aligned} CNR = {} & PWR + PKAVG + GAIN + LAMLOG \\ & + CIT + CAREA + OTH - R4TH \\ & - LOSS\ (hop\ 1) - LOSS\ (hop\ 2) - NOISE \end{aligned}$$

Table 8. RADARC clutter-to-noise radar equation

PWR	=	transmitted power
GAIN	=	sum of transmit and receive gains
LAMLOG	=	$\lambda^2 / (4\pi)^3$
R4TH	=	$1 / R^4$ loss
LOSS (hop 1)	=	non-deviative absorption + deviative absorption + obscuration (sporadic E) + auroral (where applicable)
LOSS (hop 2)	=	LOSS(hop 1) + groundloss + LOSS(hop 2)
NOISE	=	CCIR external noise (assumes 1Hz bandwidth)
CAREA	=	σ^0 times illuminated ocean area = (-29dBm / m^2)(area)
PKAVG	=	average/peak power ratio = 0 dB
OTH	=	over-the-horizon enhancement = 6 dB
CIT	=	coherent integration time

Most of these terms are familiar from the standard radar equation. It is assumed that the signal processing in the radar is approximately equivalent to a matched filter. Details of the signal processing will be described below.

The **propagation losses** are peculiar to ionospheric propagation. There is **no auroral loss** in the present comparison, because we were not looking towards the auroral regions.

The noise in Table 8 is the maximum of internal noise or external noise. The internal noise is based on measured ROTHR noise figures. The external noise is taken here to be the **CCIR external noise only**, but could also be set to include the spread-doppler clutter model already incorporated in RADARC. This **spread-doppler model** is not yet range-folded to ambiguous ranges and would contribute only when local to the radar. Since the radar is in Alaska, spread-doppler clutter from the equator would make no contribution for the two-hop propagation assumed in this analysis. RADARC can predict long range propagation to the equator, in which case the spread-doppler clutter would be included, but this is different from range-folding. When significant discrepancies in the comparison are found between predicted and measured noise, we expect to explain this primarily by invoking the spread-doppler phenomenon.

The **ocean reflectivity** σ^0 (we use a average value of 29 dBm/m^2) is calculated for an estimated average sea-state (not fully-developed, averaged over radial ocean wave velocity, averaged over polarization). We expect that the discrepancy between this assumed average reflectivity and the true reflectivity in the data will sometimes be a significant source of error in the predicted clutter. Not only may the sea surface vary from the assumed average, but also we will sometimes be looking at land, as is evident from the map in Figure 1.

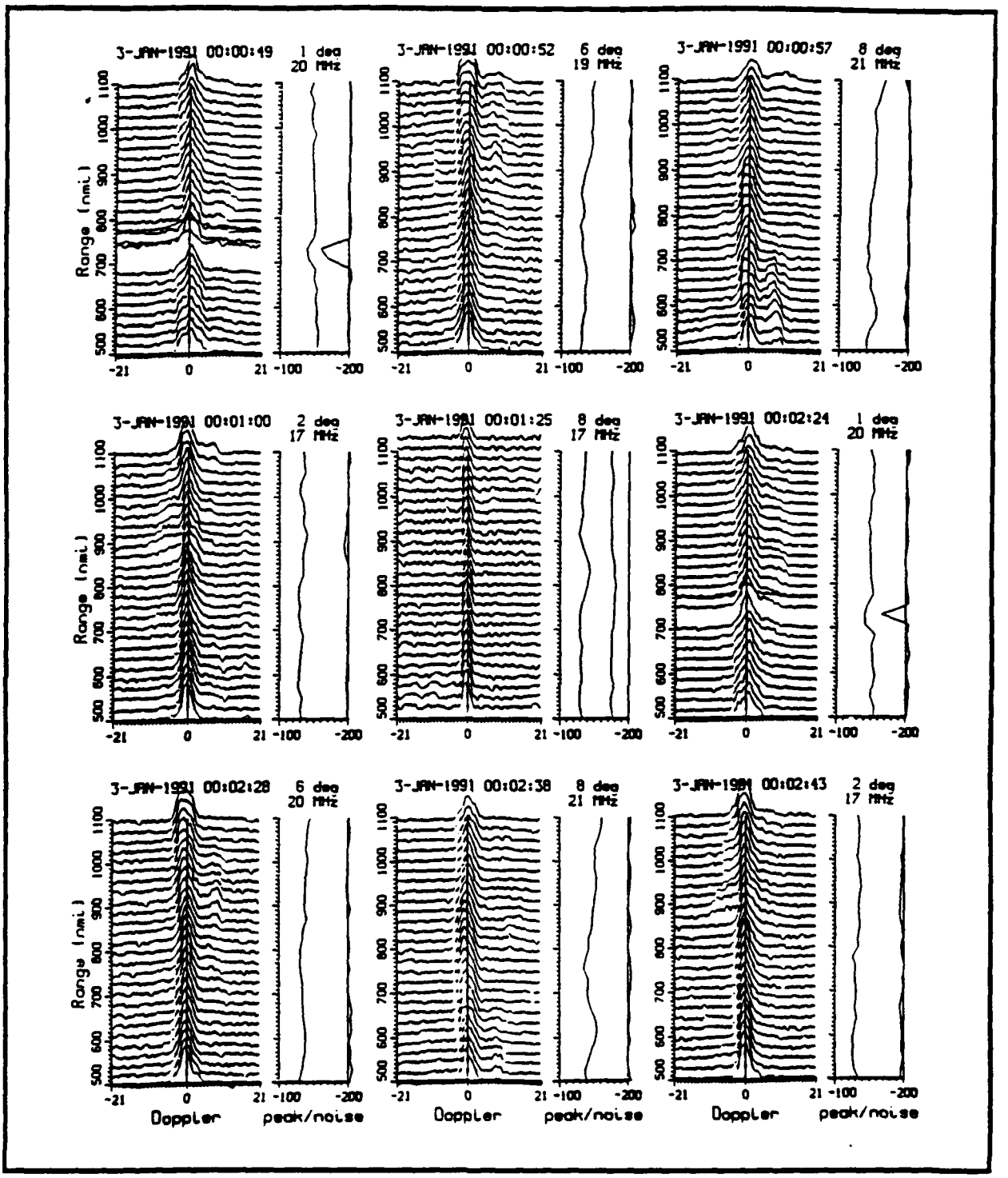

Figure 2.1 Amplitude-range-doppler maps for 0 UT (day in Amchitka), January 3, 1992. The vertical axis is range in nmi from the radar, and the horizontal axis is doppler in Hz. The ocean clutter is concentrated around 0 Hz. A median in power has been taken over 16 beams. The smaller plot shows clutter peak and noise in unscaled dBW vs. range. The noise power is the average of + and - WRF/4. The waveformcode is number 117 (see text).

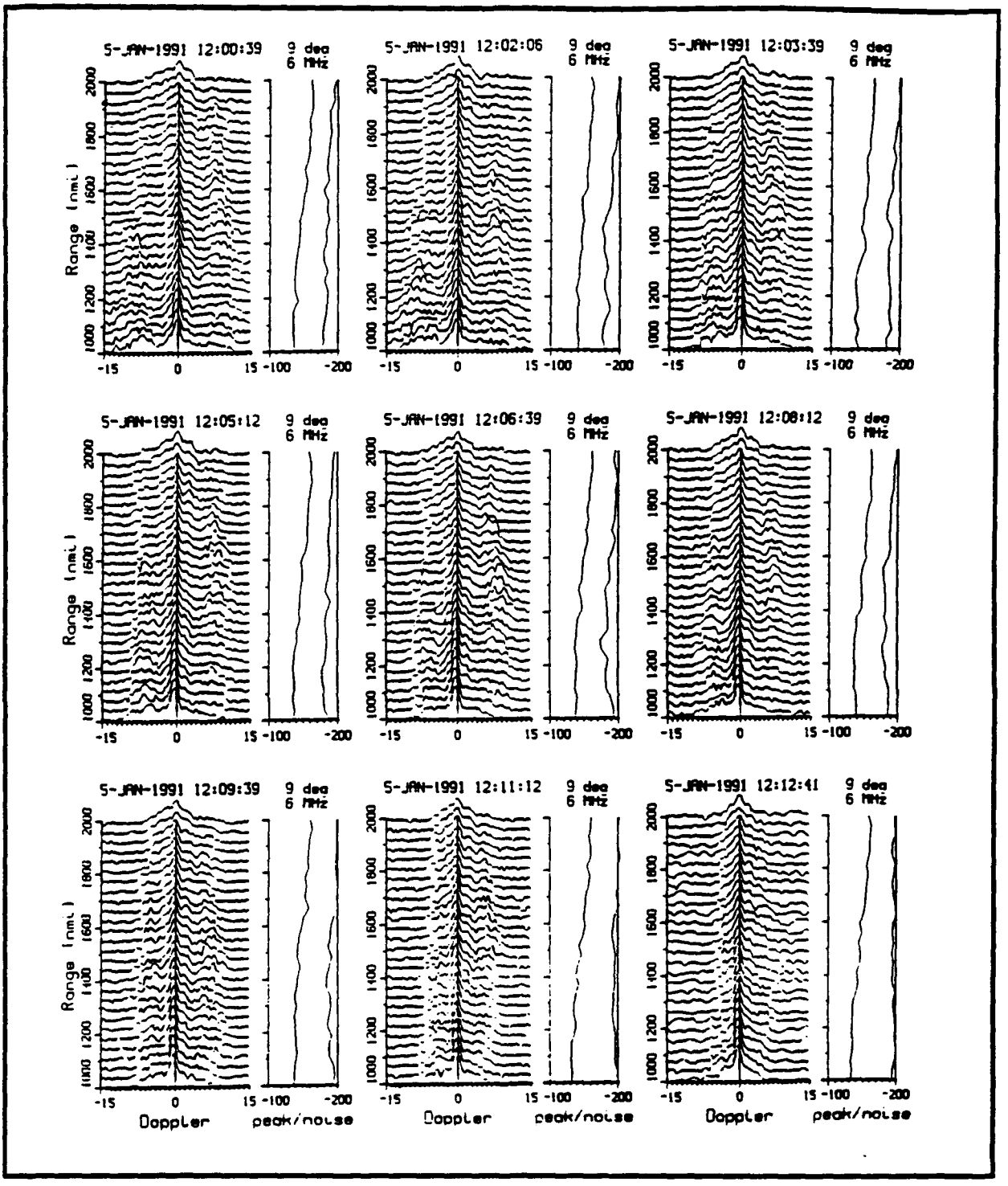

Figure 2.2. Amplitude-range-doppler maps for 12 UT (night in Amchitka), January 5, 1992. The vertical axis is range in nmi from the radar, and the horizontal axis is doppler in Hz. The ocean clutter is concentrated around 0 Hz. A median in power has been taken over 16 beams. The smaller plot shows clutter peak and noise in unscaled dBW vs. range. The noise power is the average of + and - WRF/4. The waveformcode is number 117 (see text).

The **peak-to-average power ratio** is unity because we are considering FMCW with constant amplitude. The **OTH enhancement** is a factor that accounts for multipath and the conductivity of the ocean surface. We have used 6 dB rather than the conventional 12 dB. Some other terms will be explained below, after a discussion of the signal processing in the radar.

As stated, the predicted clutter power is found by adding the predicted CNR to the CCIR noise. Some further adjustments are necessary when estimating absolute powers. In particular, the **antenna and cable losses** must be accounted for. (These cancel out in the ratio of clutter to noise and are not included in the equation above. In other words, we have replaced the customary directive gain with absolute gain. Directive gain is satisfactory when we require only CNR and the radar is externally noise-limited, so that both clutter and noise are reduced by the same factor in the antenna.) The antenna and cable losses are frequency-dependent and are shown in the following table.

Frequency	Loss	Frequency	Loss
5 MHz	21.6 dB	17 MHz	4.5 dB
6 MHz	17.0 dB	18 MHz	4.5 dB
7 MHz	13.9 dB	19 MHz	4.4 dB
8 MHz	11.7 dB	20 MHz	4.3 dB
9 MHz	10.0 dB	21 MHz	4.3 dB
10 MHz	8.7 dB	22 MHz	4.4 dB
11 MHz	7.4 dB	23 MHz	4.5 dB
12 MHz	6.3 dB	24 MHz	4.7 dB
13 MHz	5.6 dB	25 MHz	5.2 dB
14 MHz	5.2 dB	26 MHz	5.3 dB
15 MHz	4.9 dB	27 MHz	5.4 dB
16 MHz	4.6 dB	28 MHz	5.5 dB

Table 9. Antenna and Cable Losses as a Function of Frequency

Now turning to the **recorded radar data**, we must address the issue of **scaling**. The clutter and noise powers are provided by the "log-amp" data, which consists of received power vs. range and doppler expressed in decibels. This power is recorded after passing through the signal processing chain (range, azimuth, and doppler DFTs), but first it is offset by a so-called scaling factor. The scaling factor is chosen such that the values of power on tape are correct for a point-source (coherent) target (which we may call a signal) at the center antenna element. However, since we have only offset the power resulting from the entire signal processing chain, the relative values of signal and clutter, signal and noise, and clutter and noise are the same as at the output of the signal processor. In other words, the radar only "sees" relative powers, which include signal processing gains and minus the losses. Naturally, the "growth" of the coherent part of the data is greater than for the incoherent part, which is how we get the signal-to-noise and signal-to-clutter gains necessary to detect targets. The signal processing growths (excluding losses) of the various data components are as follows:

INPUT	RANGE DFT	AZIMUTH DFT	DOPPLER DFT
Clutter	WRF/BW_{RX}	$N_{EL}^2 \times (\theta_{RX}/\theta_T)$	1
Signal	1	N_{EL}^2	1
Noise	WRF/BW_{RX}	N_{EL}	$1/(WRF \times CIT)$
CNR	1	$N_{EL} \times (\theta_{RX}/\theta_T)$	$WRF \times CIT$
SNR	BW_{RX}/WRF	N_{EL}	$WRF \times CIT$

Table 10. Signal processing gains (excluding losses)

WRF	=	Waveform Repetition Frequency
BW_{RX}	=	Receiver Bandwidth
N_{EL}	=	Number of active elements
θ_T	=	Transmit beamwidth
θ_{RX}	=	Receive beamwidth
CIT	=	Coherent Integration Time

The receive antenna gain is obtained in the azimuth DFT. Each element has its own receiver and all three transforms are performed in the digital (software) domain. Although conceptually it does not matter in which order we perform the three DFTs, the hardware is designed such that a range DFT is applied to the output of each separate receiver before they are all combined in the azimuthal DFT. Finally the doppler DFT is taken, power is extracted, and any scaling is applied. The range and doppler DFTs are normalized such that the coherent power receives unity gain and the incoherent (noise) power is reduced by the ratio of the DFT cell size to the noise bandwidth of the incoming signal. In the azimuthal DFT, on the other hand, the noise grows by the number of elements (or DFT points) and the coherent power grows by that number squared. In both cases, the gain of the coherent power with respect to the incoherent power is the same; the difference is in the normalization. Further remarks on the signal processing are provided in the following paragraphs.

In the **range DFT**, the clutter is treated like noise, because different patches of ocean surface at different ranges are independent so that no phase relationship between them is preserved in the Bragg scattering. The WRF gives the range DFT cell size or resolution because it is the inverse of the duration of the chirp. The bandwidth of the receiver determines the bandwidth of the noise before the DFT is applied.

In the **azimuth DFT**, the clutter in any one azimuthal direction is treated as coherent (with an N^2 factor), because we have far-field plane waves impinging on the array. But now this backscatter-dependent power is reduced by the ratio of receive to transmit beams. (The power is incoherent between different azimuthal cells for the same reason as in the range processing.) The noise, on the other hand, is assumed decorrelated between elements and isotropic (this last assumption may not correspond to reality) so that its gain is the customary N, where N is the number of DFT points, for a normalization such that coherent power is increased by N^2.

Finally, in the **doppler DFT**, both signal and clutter are assumed coherent (the ocean clutter is usually coherent to first order over time at a given range), so that the SNR and CNR gains are both equal to the number of samples, which is the same as WRF times CIT (the CIT is the duration of all chirps in the waveform and we get one doppler sample at each range in each chirp). These signal processing gains must be adjusted for windowing, scalloping, and other losses, which total about 9 dB for the entire signal processing chain.

These signal processing gains indicate how we should adjust the recorded data to get agreement with the RADARC prediction. RADARC predicts the clutter and noise as observed by the radar after the signal processing chain. The data is scaled to a coherent target at the center element, but the relative powers of the different parts of the doppler spectrum are as observed by the radar. That is, the scale factor was chosen to subtract the processing gain of the coherent power, which from Table 10 is equal to the azimuthal DFT (array) gain only, as the range and doppler gains are unity for the signal. (The SNR increase in the range and doppler DFTs results from *reduction* of the noise power.) The array power gain is N^2, where N is the number of array elements, which varies with frequency. For the amplitude, we take N instead of N^2. Of course, we must adjust this antenna gain for the Taylor windowing losses. The compensated array gains are shown in the following table versus frequency.

Frequency	Elements	Array Gain	Windowing loss		Compensated Gain
5-16 MHz	372	25.7 dB	- 1.2 dB	→	add 24.5 dB to data
16-20 MHz	300	24.8 dB	- 1.2 dB	→	add 23.6 dB to data
20-24 MHz	244	23.9 dB	- 1.2 dB	→	add 22.7 dB to data
24-28 MHz	202	23.1 dB	- 1.2 dB	→	add 21.9 dB to data

Table 11. Adjustment to data for array gain

4b. Description of Software

We have received a very large number of ROTHR data tapes from Amchitka. Our first task was to archive the data on the 9-track radar tapes to a more convenient 8-mm format. Then we extracted the desired data from the 8-mm tapes and recorded it to a convenient database on the computer, namely, a large disk file that can be easily accessed when we want to look at the data in different ways. We refer to this operation as the "processing" of the ROTHR data tapes.

The database is organized by month and hour. One hour of one day is processed at a time, as the ROTHR tapes are the actual real-time record of the radar operation. The processing involves extracting the "log-amplitude" data (i.e. received power vs. range and doppler) from all the data recorded. This log-amplitude data is recorded in units called dwells, since the radar scans over a large coverage area, illuminating one specific region at a time (for example, see Figures 2.1 and 2.2.). The data for the same hour on different days are accumulated to reduce the variance in the clutter and noise associated with any given day. Our final goal is to obtain measures of average clutter and noise power for each geographical region of interest for certain hours of the day in each of the selected months, and compare this with the RADARC prediction based on monthly medians. When we average the data, we will use the median* rather than the linear average, so as to reduce "outliers" or other unusual circumstances which skew the data.

* We mean median in the usual sense: in a given data set, half the values are greater than or equal and half are less than or equal. If the number of data points is even, the lesser of two possible medians is chosen, although this technicality is trivial.

The ROTHR log amp data as recorded on tape is scaled to a reference point, namely the input to the receiver of the center element (specifically to the point where the cable from the twerp** feeds the attenuator in front of the receiver). This scaling is correct only for a point source target. In order to effect the comparison with RADARC, we must undo this scaling as described in the previous section.

Two computer programs are used in the analysis. This first is called Q4202. It reads the log-amplitude data on the ROTHR tapes, one dwell at a time, averages this data over azimuth (i.e. beams) and range as described below, determines clutter and noise, and records these "data points" to a database. The second program is called QBASE. It reads the database, selects a set of ROTHR data points according to various criteria (month, hour, waveform code, range, frequency, azimuth), adds specified offsets and correction factors (if any), and plots these points along with the RADARC prediction. There are various plot formats. One is a scatter plot of ROTHR data points vs. RADARC predicted values (not shown in this report). Another plots the ROTHR data and RADARC prediction vs. range for specified frequency intervals. Figure 5.1 is an example of the latter.

When program Q4202 reads the ROTHR tapes, it first reads in information from the tape headers. This includes TOA (Time of Action - both date and universal time), frequency, RWST (Range Window Start Time - which is multiplied by c/2 to give the slant range to the first range cell), the number of range cells, the swept bandwidth (which gives the range cell resolution), the range extent of the dwell, the number of doppler cells, WRF (Waveform Repetition Frequency - which gives the extent of the doppler axis), the number of beams, beam direction, beam width, and the beam spacing. The present analysis concentrates on waveform code 117 (the most common one), although it is sometimes necessary to consider waveform code 173 in order to get enough data points for a particular case.

Waveform code 117 has the following parameters:

- number of range cells: 53
- range extent: 953.2 km (514.7 nm)
- range cell resolution: 17.99 km (9.71 nm)
- number of doppler cells: 128
- WRF: 42.0 Hz
- CIT: 3.1 seconds,

and **waveform code 173** has the following parameters:

- number of range cells: 55
- range extent: 989.2 km (534.1 nm)
- range cell resolution: 17.99 km (9.71 nm)
- number of doppler cells: 128
- WRF: 31.0 Hz
- CIT: 4.1 seconds.

To run program Q4202, a headers file must first be generated with program A4202. This headers file contains the TOA's of all the log amp dwells on a particular data tape, along with the WFC, frequency, start range (from RWST), and beam parameters.

Then the tape is processed with program Q4202. A waveform code, month, and hour of the day must first be selected. A list of all available dwells satisfying these parameters is then generated by reading the headers file. To reduce the amount of data to a manageable level, only those azimuths within 20 degrees of boresight are retained. A further decimation of the data is

** A pair of endfire monopoles

achieved by selecting an arbitrarily chosen (10 in our case) maximum number of dwells from those azimuths. It is better not to have, say, 100 dwells from one azimuth and 10 from another, as we would then get a statistically biased database. Since each tape covers about half an hour, we get up to 20 dwells per azimuth per hour per day. Each dwell provides about 5 clutter and 5 noise points, after we average over a 97 nm range window (see below). This gives up to 100 clutter and 100 noise points per azimuth per hour per day. With 10 days of data per month, we get up to 1000 clutter and 1000 noise points per azimuth per hour per month. This should adequately represent the performance of the radar.

The program now has a list of dwells for the data tape being processed. It begins to read and process these dwells sequentially. In each dwell, it first averages over about 8° of azimuth by taking the median over the 16 beams at each range-doppler cell. (Taking the median eliminates "outliers" which would be included if we took, say, a linear average.) Then an average (median) is taken over groups of 10 range cells (at each doppler cell) to further smooth the data. Thus the average in range is over 97 nm for the waveform codes chosen here. For any dwell, we now have a set of doppler clutter spectra that are averaged over beams and range. The program then determines noise and clutter at each of these averaged doppler spectra. This is repeated with each of the selected dwells and is recorded to the database. The whole process is repeated with each tape. The steps in this processing can be summarized as follows.

- The raw data consists of amplitude-range-doppler maps

- Step 1: Take median power over 16 beams at each range-doppler cell of dwell
- Step 2: Take median power over 100 km range at each doppler cell (~5 range cells)
- Step 3: "Clutter" is maximum power in a small window around 0 Hz.
- Step 4: "Noise" is dB average of power at + and - WRF/4.

- Each of these clutter and noise samples shows up as a tiny black dot on the plot
- Open circles are the medians of black dots with 100 nm intervals (e.g. 700-800 nm)

Table 12. Algorithm for extracting clutter and noise from raw data.

When program QBASE reads the ROTHR database, it also makes a comparison with the prediction from RADARC. Before processing the ROTHR tapes, the necessary output must first be generated with RADARC and recorded. For a given month, hour, and azimuth, RADARC provides (among other output) a CNR (clutter-to-noise) map vs. slant range and frequency. A complete list of inputs to RADARC is shown in Table 13.

A CNR map is generated for each degree of azimuth between -20 and +20 degrees with respect to boresight and is recorded. This map also contains the CCIR noise, and so we can determine clutter power by adding the CNR to the noise. Each map is a grid of CNR at discrete points vs. frequency and slant range. The frequency is in 1 MHz increments and the slant range is in 80 nm (148 km) increments. When QBASE reads this map to make a comparison, it interpolates on the map at the same frequency and slant range as the ROTHR data point currently being examined. The new version of RADARC (2.0) has been used for all data processed in this report. It tries to correct defects in the old version (1.0), particularly with respect to the statistical databases. Corrections can also be inserted in the processing done by QBASE. Examples of this include antenna and cable losses not accounted for in RADARC and the ROTHR tape scaling described above.

When we generate a plot from the ROTHR database, we can select intervals of frequency, range, and azimuth. This simplifies the analysis by focusing on some narrow parameter region over which some of the factors affecting the data are expected to remain constant. In particular, we have geogr .phy in mind, as described in the Introduction. It is also important to consider a narrow frequenc band, as many of the components of the CNR equation vary considerably with frequency.

- month, hour, and azimuth
- sunspot number (taken from the Solar Indices Bulletin published by the National Geophysical Research Center). The smoothed sunspot numbers for 1991, at the time the analysis was performed, were: 148 for January, 147 for April, and 136 for July.
- transmitter location (Amchitka is at 51.44 N and 179.16 E)
- transmitter power (200 kW)
- the ionospheric layer corrective multiplicative factors (nominal values kept)
- the interference noise level in Amchitka for 1 Hz BW (nominal value 204.0 kept)
- range resolution (200 μs)
- average-to-peak power ratio (nominal value of 0 dB kept)
- the OTH path enhancement (nominal 6 dB kept)
- CIT (set at 3.1 s to match WFC 117 or 4.1 s for WFC 173)
- the multiplicative factor for deviative absorption (nominal 1.0 for hops 1 and 2 kept)
- the type of noise (selected to be the maximum of the ROTHR noise curves or of the galactic and atmospheric noise from CCIR 322)
- the vertical radiation increment (nominal 1.0 degrees kept), and
- the antenna type (selected to be ROTHR short ground screen).

Table 13. Input parameters to RADARC model

4c. Discussion

The comparison between the RADARC predicted clutter and noise and the ROTHR data is shown in the **figures of Appendix C**. There are two sets of figures, which both show the same data in different ways. The first set (Figures 5.1 to 5.10) shows the ROTHR clutter and noise power vs. range as dots and the RADARC model comparison as solid curves. (The open circles are median powers over range.) The second set (Figures 6.1 to 6.6) shows the median powers of the ROTHR data and of the model over selected range, frequency, and day intervals.

In the **first set of figures**, each figure shows the RADARC prediction and the ROTHR data for a specific hour and month, as indicated at the top. The solid curves are the RADARC predicted clutter and noise powers, and the tiny black dots are the ROTHR data. The open circles are the medians of the ROTHR data over 100 mile intervals, as discussed above. Each subplot represents the data from a 1 MHz band. Of course, many of the 1 MHz bands have little or no data,

indicating that these were not good operating frequencies at the time and were therefore not selected by the radar operators.

Essentially all we want to determine is how well the data points near the top (the clutter) cluster along the RADARC prediction and how well the data points at the bottom (the noise) cluster along the flat curve representing the RADARC predicted noise. The difference between individual data points and median data points should be kept in mind, as the individual data points (representing individual dwells) will tend to have much more variability than medians (unless there were few data points available in the estimate of the median).

Note that the actual days of the month represented by the ROTHR data points are indicated along the tops of the subplots. The RADARC frequency is also indicated; it is always the starting frequency of the 1 MHz band (e.g. 8 MHz for the 8-9 MHz band). The number of individual data points contained in the median estimate points is indicated along the bottoms of the subplots underneath the corresponding open circle representing the median estimate.

The **second set of figures** in appendix C shows median dB powers of the data and the model vs. range, frequency, and day. For example, in the case of range, all the data points for a given month and hour were sorted into 100 mile bins, the first from 500 to 600 miles (slant range), the second from 600 to 700 miles, and so on up to 2000 miles. The median clutter and noise powers were then found in each bin for both the data and the model. Note that each bin contains all points at a given range, regardless of frequency or day.

A similar procedure was followed for frequency and day. In the case of frequency, the bins were 1 MHz wide, from 5 to 28 MHz. All data points of a given frequency, regardless of range or day were placed in the corresponding bin and the median power taken. In the case of day, all data points from a given day of the month, regardless of range or frequency were placed in the proper bin and the median power taken.

This procedure obviously provides additional insight into the source of errors. For example, if for a given month and hour there is a large error at a certain frequency and also for a certain day, then we may suspect some connection and this will guide us in taking a detailed look at the data. Better yet would be some display that shows correlations in error between range, frequency, and day.

Due to the spread-doppler clutter problem, the **noise measurements** are of particular interest. Recall that the RADARC predicted noise is CCIR ambient noise (without a folded spread-doppler clutter estimate). Therefore, when range-folded spread-doppler clutter is present, we would expect the ROTHR noise to exceed significantly the RADAR noise. We would expect this to occur especially at night (hour 12 UT).

The following tables presents the dB difference between the powers of the ROTHR measured noise and the RADARC predicted noise for all the data presented in Appendix C. The columns are the operating frequencies in MHz, as indicated by the numbers along the top. The rows are the month, as is evident from the labels at the left. The top table is the daytime noise difference (00 UT), and the bottom table is the nighttime noise difference (12 UT). The bold numbers indicate differences between data and model that exceed 10 dB.

Indeed, the nighttime noise differences are significantly larger than for daytime, although January day is rather high. The nighttime noise for July was especially high. It should be remembered than all of the data presented in this report was restricted to a 10° azimuthal sector, and therefore does not represent an isotropic average.

The spectrum monitor data do not show noise levels that depart significantly from that of CCIR or internal noise [5]. Therefore we conclude that the high noise levels are due to clutter spread in Doppler.

Noise difference DAY (00 UT)

Freq	5	6	7	8	9	10	11	12	13	14	15	16	17	18	19	20	21	22	23	24	25	26	27
JAN						5	2			2	6	3	7	7	7	7	6	12	11	10	11	15	
APR						0	-1	-3	-2	1	0	-3	-1	2	1	1	2	3	3	2	3	5	1
JUL									-3	-2	-2	-4	-3	-1	-2	-3	-3	-2	-2	-4			

Frequency in MHz.

Noise difference NIGHT (12 UT)

Freq	5	6	7	8	9	10	11	12	13	14	15	16	17	18	19	20	21	22	23	24	25	26	27
JAN	10	9	6	5	2																		
APR										11	7	6	6	5		10	5	*	*	*			
JUL					18			18	18	17	11	8	16	20									

Table 14. Noise power difference in dB of ROTHR median and RADARC prediction

For the clutter, we present a table of dB power differences vs. range rather than frequency. In the case of clutter, we assume that the operating frequency is optimized for a given range, and we are more interested in the significant differences in clutter power vs. range that occur due to the changes is propagation path and surface reflectivity. The bold numbers indicate differences between data and model that exceed 10 dB. (These values are averaged over frequency.) Again, this table summarizes the data in Appendix C.

Clutter difference DAY (00 UT)

Range	500	600	700	800	900	1000	1100	1200	1300	1400	1500	1600	1700	1800	1900
JAN	-4	**-12**	**-12**		-6	**-12**	-9	9	-1	1			1	1	-4
APR	**-10**	-2	-2	**11**		-13	-9		**-17**	**-13**	**19**	-2	-1	-1	3
JUL	2	**11**	**13**	8	4	**-13**			**-14**	**-15**	**-15**		**26**	**23**	**35**

Range in nmi

Clutter difference NIGHT (12 UT)

Range	500	600	700	800	900	1000	1100	1200	1300	1400	1500	1600	1700	1800	1900
JAN	-5	-3					-5	-3	-3	-4			**-10**	3	5
APR										**21**	8	-8	-5	**20**	4
JUL	3	-7			-8	-4	-8		0	3	-4			**11**	**22**

Table 15. Clutter power difference in dB of ROTHR median and RADARC prediction

The analysis of the clutter is more qualitative and therefore more subjective. The following table presents a summary of our evaluation of the data presented in Appendix C.

Median Signal Level Comparison

- Generally adequate considering the limitations on our knowledge of the antenna patterns, sea-scattering coefficient, median ionospheric parameters, etc.
- Distribution of levels (variability) about as expected from previous analysis of one-way data
- Another source of error, as shown by the WSBIs, is that significantly more sporadic E occurred than was predicted.
- No consistent bias.

Median Noise Level Comparison

- Good day time agreement
- Nighttime levels higher than model due in part to spread-doppler clutter.

Table 16. Summary of analysis of amplitude vs. range.

5. Conclusions

For three seasons, ten days, noon and midnight, we have examined the vertical ionograms, the widesweep backscatter soundings, the radar's earth backscatter levels, and the ambient noise. These data have been compared with the RADARC Model predictions. In Appendices A, B, and C the data and predictions are available for detailed examination.

Electron Density Distributions. The median of the observed vertical ionograms has been compared with the RADARC model. The emphasis was on the critical frequencies. Heights were also compared to a lesser extent. A simple algorithm was devised to permit computer comparison in addition to the comparison from manually drawn families. The model F_2 layer critical frequencies are mostly within 0.5 MHz of the observed median, and in general the model shows agreement with the data. The April day data appears to straddle both winter and spring conditions; it would be interesting to examine the Fall data. There are indications that some adjustment in model layer heights and thicknesses might improve the model. The simple algorithm for machine analysis of median ionograms can and should be improved if more detail is desired. We feel that, in general, any improvement in model electron distributions will have only a small impact on predicted performance.

Wide Sweep Backscatter Ionograms (WSBI). These oblique earth backscatter soundings should provide the best data for comparison with model performance prediction. WSBI intensity-range-frequency plots are compared with RADARC plots in a qualitative manner. The skip zones can be compared on an absolute basis, and they are very similar. Since the times used are near midday and midnight, there were probably no severe horizontal electron density gradients, and consequently the deficiencies in RADARC's treatment of "tilts" are not exposed. Further investigation will examine sunrise and sunset for the same ROTHR database as was used in this report.

Radar Ground Backscatter Levels. Appendix C Figure 6, the amplitude versus range plots provide a good comparative view between prediction and observation. Some of the disagreement is certainly due to our assumption of a constant surface scattering coefficient. There appears to be a slight optimistic bias by the Model which is due in part to the existence of more sporadic E ionization than was predicted. However, considering the complexity of the ionosphere and of the propagation, and the fact that we are trying to predict these events from a statistical database with no reliance on auxiliary real-time measurements, the comparison between signal levels (clutter) from the RADARC model and the ROTHR data is fairly good.

Noise. The Appendix C Figure 6 noise level versus frequency curves give a comparison in familiar form. Actual noise is higher than the Model at night for all seasons and is also higher by day in January. Examination of amplitude-range-Doppler maps shows this discrepancy to generally be due to "multiplicative" noise; that is, noise that disappears when the transmitter is turned off and which comes from clutter spread out in Doppler.

The major deficiency exposed in RADARC is due to radar noise levels that are higher than those due to atmospheric, galactic or internal noise. These generally occurred at night and during some January days. We feel that an improvement in performance prediction requires an improved ionospheric irregularity model since this is the source of spread doppler clutter. Equally important, path tracing techniques must be incorporated that permit folding-in range-ambiguous and azimuthal sidelobe spread clutter. We have work underway that addresses these improvements.

References

[1] J.M. Headrick, J.F. Thomason, D.L. Lucas, S.R. McCammon, R.A. Hanson and J.L. Lloyd, *Virtual Path Tracing for HF Radar Including an Ionospheric Model*, NRL Memorandum Report 2226, March 1971

[2] J.F. Thomason, John Lloyd and Glenn Skaggs, *A Global Ionospheric Model*, NRL Report 8321, August 1979

[3] CCIR (International Radio Consultative Committee): *World Distribution and Characteristics of Atmospheric Radio Noise*, CCIR Report 322, International Telecommunications Union, 1964

[4] A.D. Spaulding and J.S. Washburn, *Atmospheric Radio Noise: Worldwide Levels and Other Characteristics*, NTIA Report 85-173, National Telecommunications and Information Administration, April 1985

[5] G.D. McNeal, *Characteristics of High Frequency Signals, Noise, Availability and Duration of Bandwidths Based on ROTHR Amchitka Spectrum Measurements*, NRL Report 9536, *under publication*

Appendix A

Comparison of RADARC Predicted Quasi-Vertical Ionograms and ROTHR Median Observed Ionograms

Figures 3.1 to 3.6

Hours 00 UT and 12 UT
January, April, and July, 1991

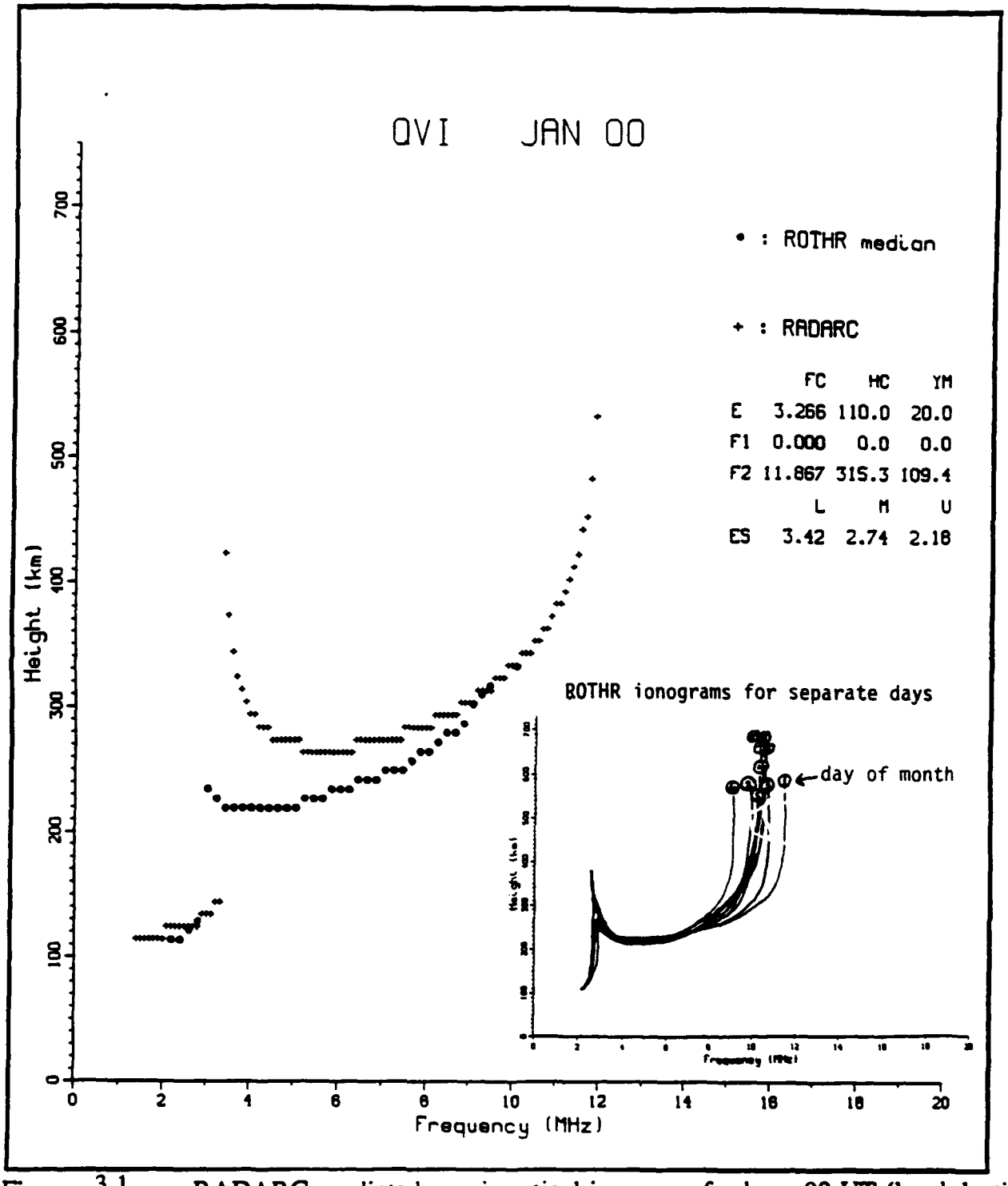

Figure 3.1 RADARC predicted quasi-vertical ionogram for hour 00 UT (local daytime) of January vs. the monthly median of ROTHR observed ionograms. The RADARC prediction is based on an estimated monthly median overhead ionosphere. On each individual ROTHR ionogram, the trace is taken to be the maximum power over height at each frequency. The median height of all traces is then taken at each frequency. This plot is based on about 40 to 45 ROTHR traces or about ten days of data.

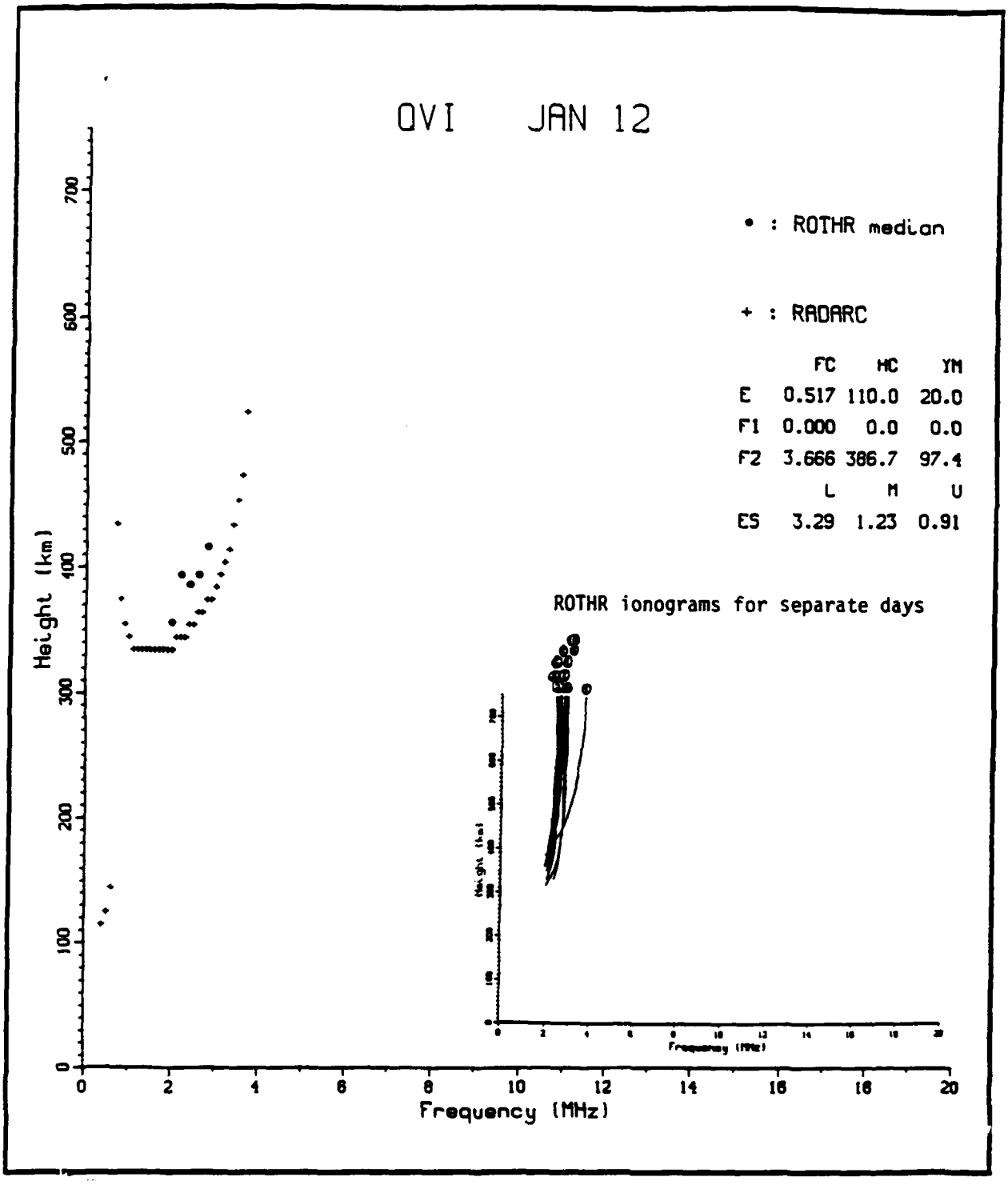

Figure 3.2. RADARC predicted quasi-vertical ionogram for hour 12 UT (local nighttime) of January vs. the monthly median of ROTHR observed ionograms. The RADARC prediction is based on an estimated monthly median overhead ionosphere. On each individual ROTHR ionogram, the trace is taken to be the maximum power over height at each frequency. The median height of all traces is then taken at each frequency. This plot is based on about 40 to 45 ROTHR traces or about ten days of data.

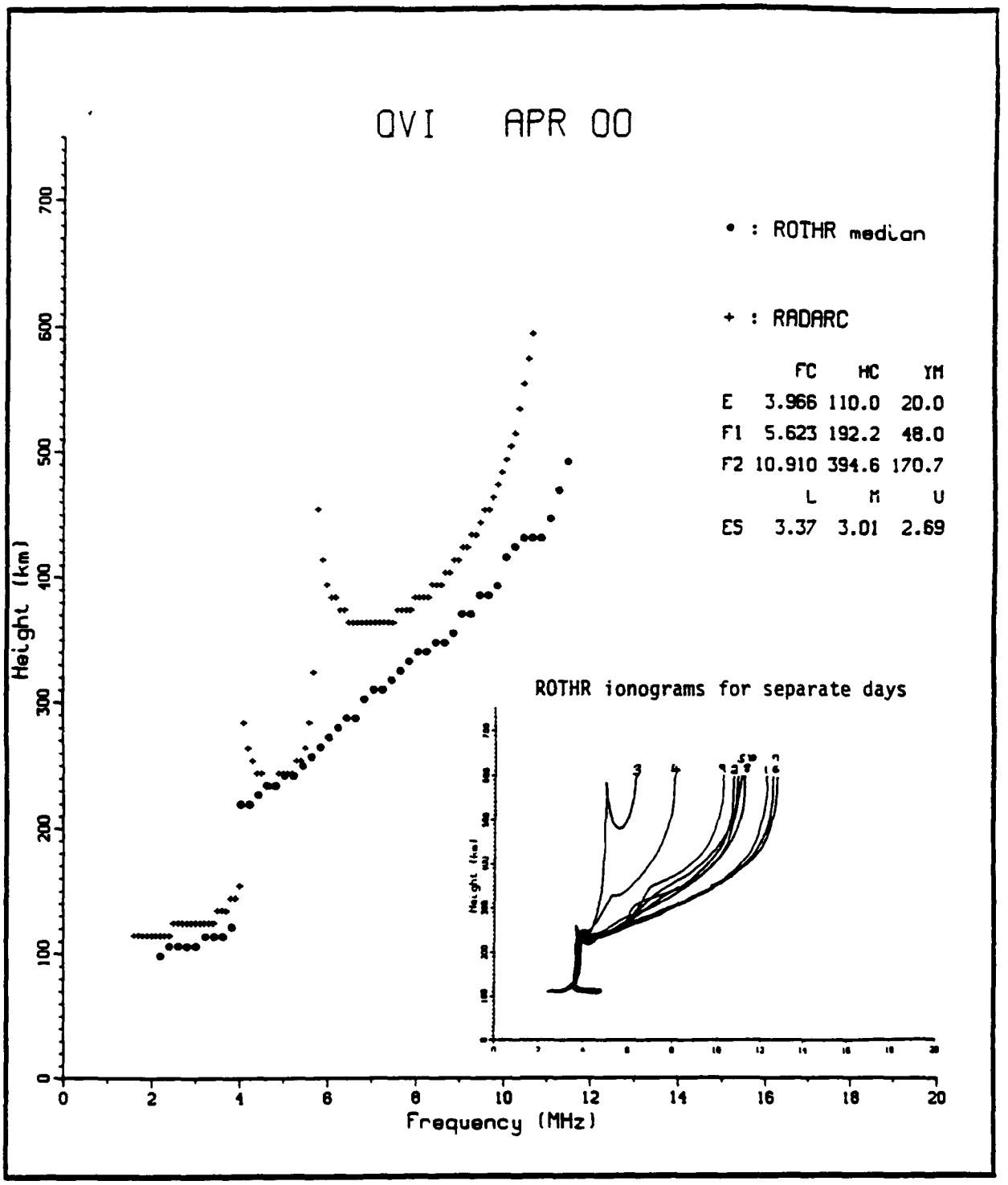

Figure 3.3. RADARC predicted quasi-vertical ionogram for hour 00 UT (local daytime) of April vs. the monthly median of ROTHR observed ionograms. The RADARC prediction is based on an estimated monthly median overhead ionosphere. On each individual ROTHR ionogram, the trace is taken to be the maximum power over height at each frequency. The median height of all traces is then taken at each frequency. This plot is based on about 40 to 45 ROTHR traces or about ten days of data.

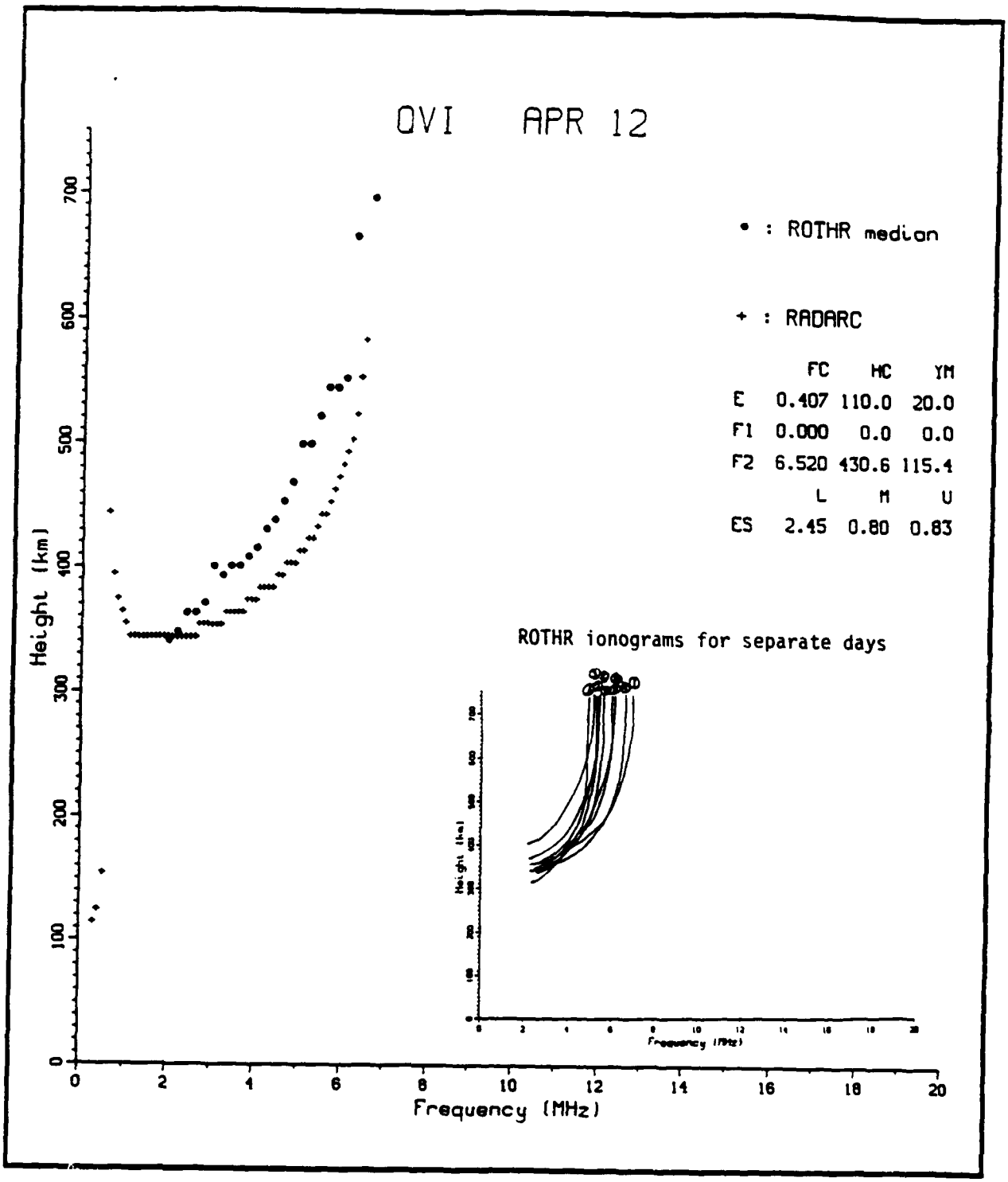

Figure 3.4. RADARC predicted quasi-vertical ionogram for hour 12 UT (local nighttime) of April vs. the monthly median of ROTHR observed ionograms. The RADARC prediction is based on an estimated monthly median overhead ionosphere. On each individual ROTHR ionogram, the trace is taken to be the maximum power over height at each frequency. The median height of all traces is then taken at each frequency. This plot is based on about 40 to 45 ROTHR traces or about ten days of data.

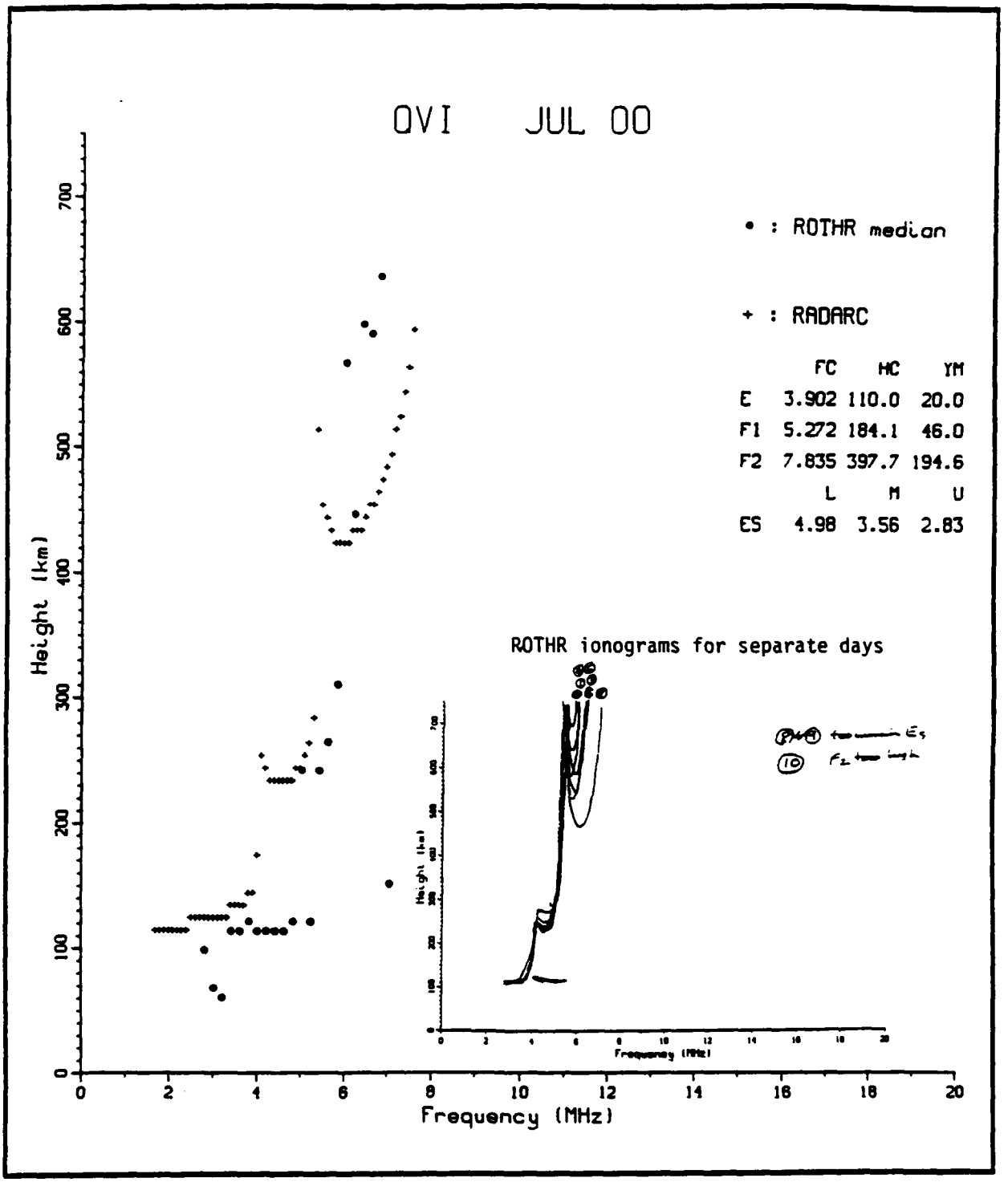

Figure 3.5. RADARC predicted quasi-vertical ionogram for hour 00 UT (local daytime) of July vs. the monthly median of ROTHR observed ionograms. The RADARC prediction is based on an estimated monthly median overhead ionosphere. On each individual ROTHR ionogram, the trace is taken to be the maximum power over height at each frequency. The median height of all traces is then taken at each frequency. This plot is based on about 40 to 45 ROTHR traces or about ten days of data.

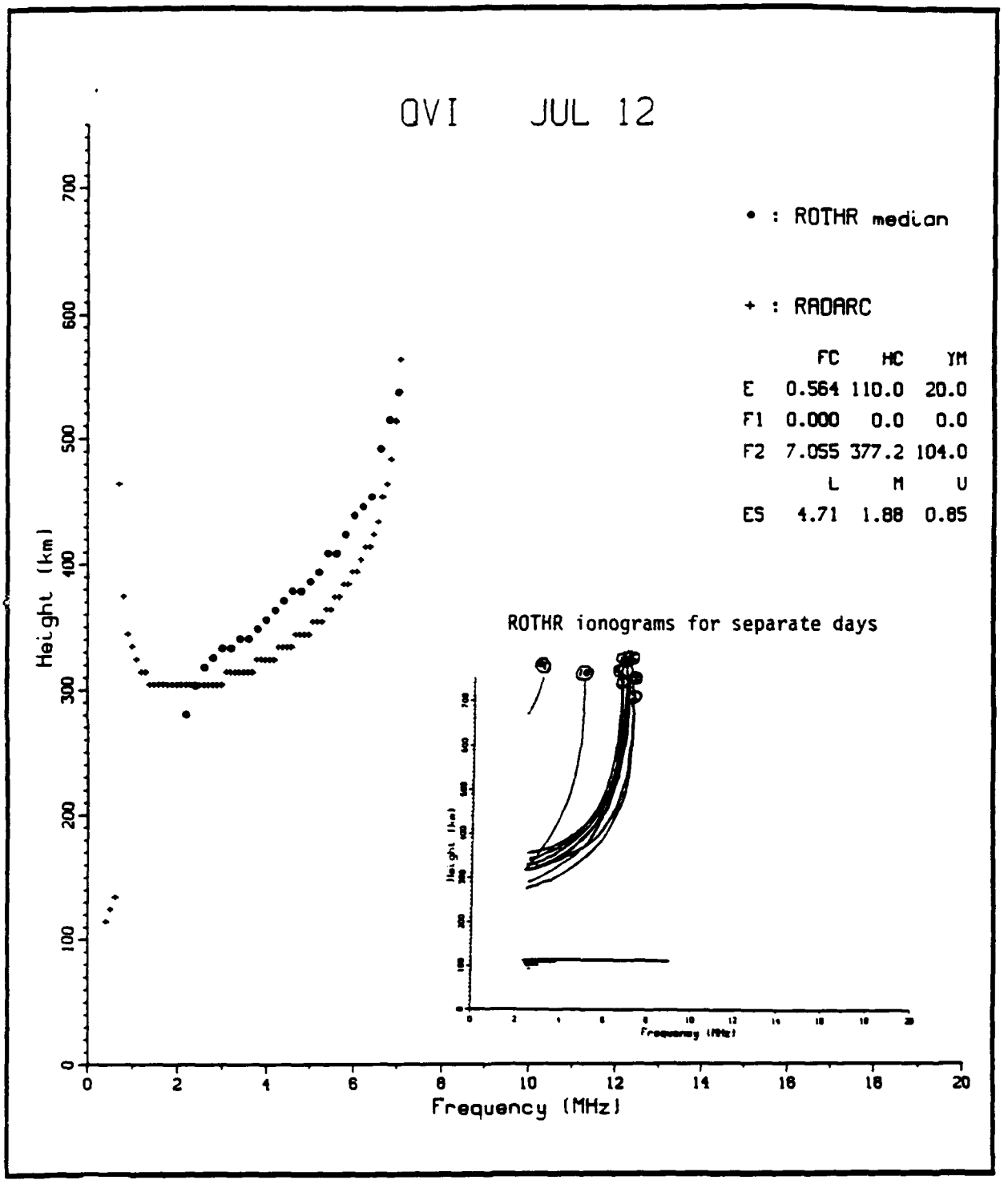

Figure 3.6. RADARC predicted quasi-vertical ionogram for hour 12 UT (local nighttime) of July vs. the monthly median of ROTHR observed ionograms. The RADARC prediction is based on an estimated monthly median overhead ionosphere. On each individual ROTHR ionogram, the trace is taken to be the maximum power over height at each frequency. The median height of all traces is then taken at each frequency. This plot is based on about 40 to 45 ROTHR traces or about ten days of data.

Appendix B

Comparison of RADARC Clutter-to-Noise Maps and ROTHR Widesweep Backscatter Ionograms

Figures 4.1 to 4.6

Hours 00 UT and 12 UT
January, April, and July, 1991

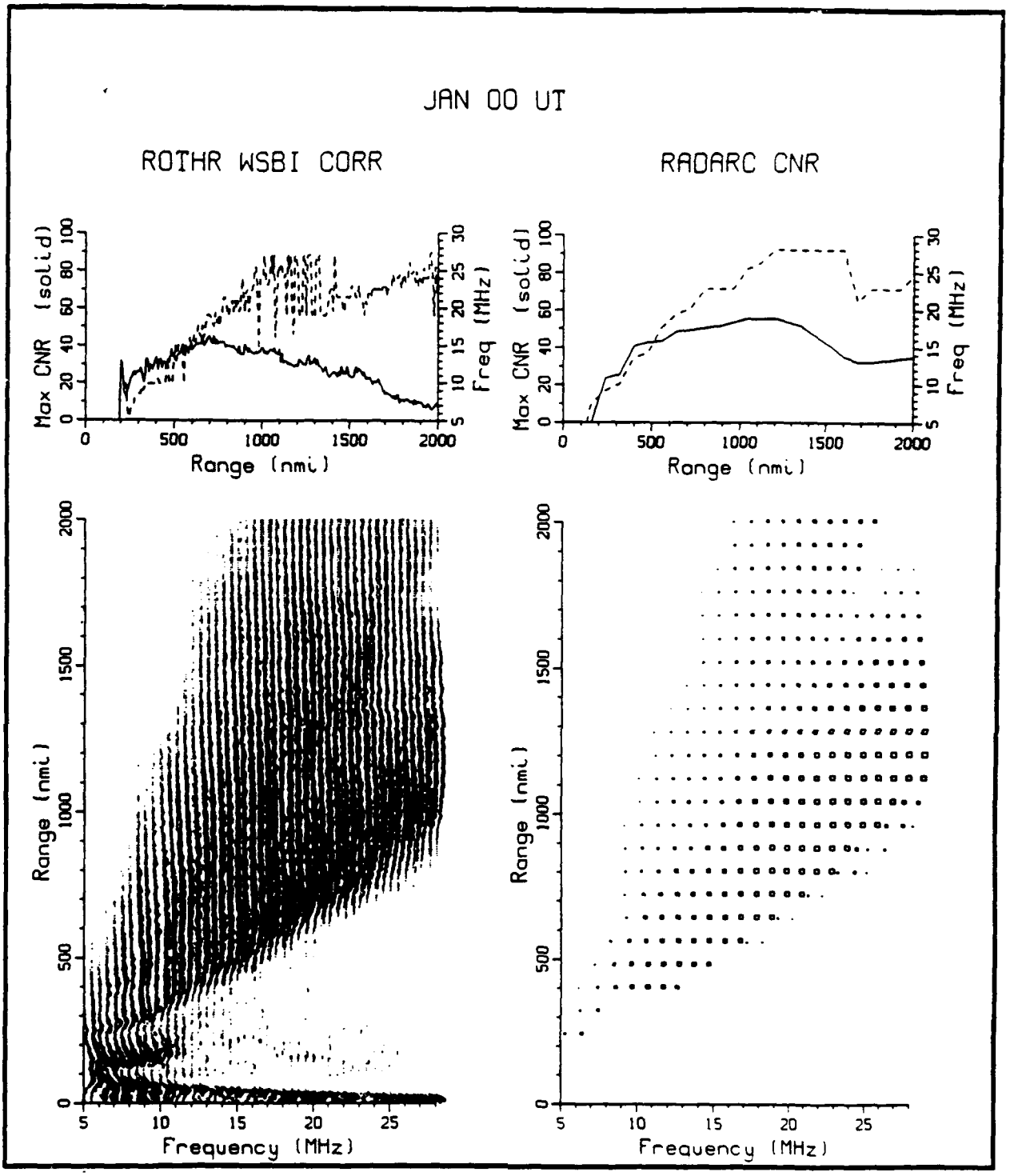

Figure 4.1. ROTHR widesweep backscatter ionogram (WSBI) vs. RADARC clutter-to-noise (CNR) map for 0 UT (noon in Amchitka) of January, 1991. The WSBIs shown here are each the average in power over about 45 individual WSBIs recorded during the first 10 days of the month. *The values in each frequency-range cell are averaged separately.* The CNR map is not expected to be identical to the WSBI, but should at least have a similar shape.

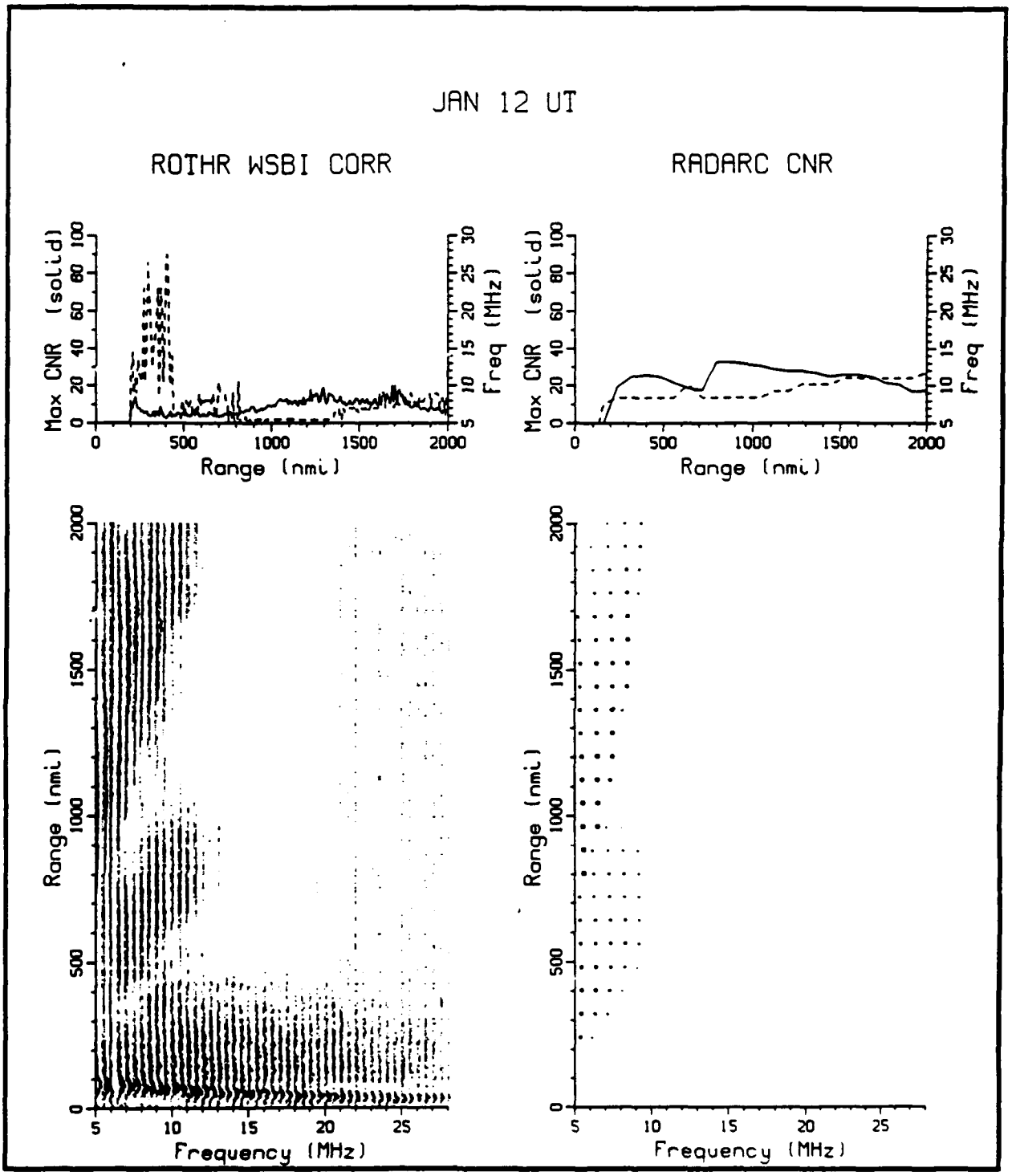

Figure 4.2. ROTHR widesweep backscatter ionogram (WSBI) vs. RADARC clutter-to-noise (CNR) map for 12 UT (midnight in Amchitka) of January.

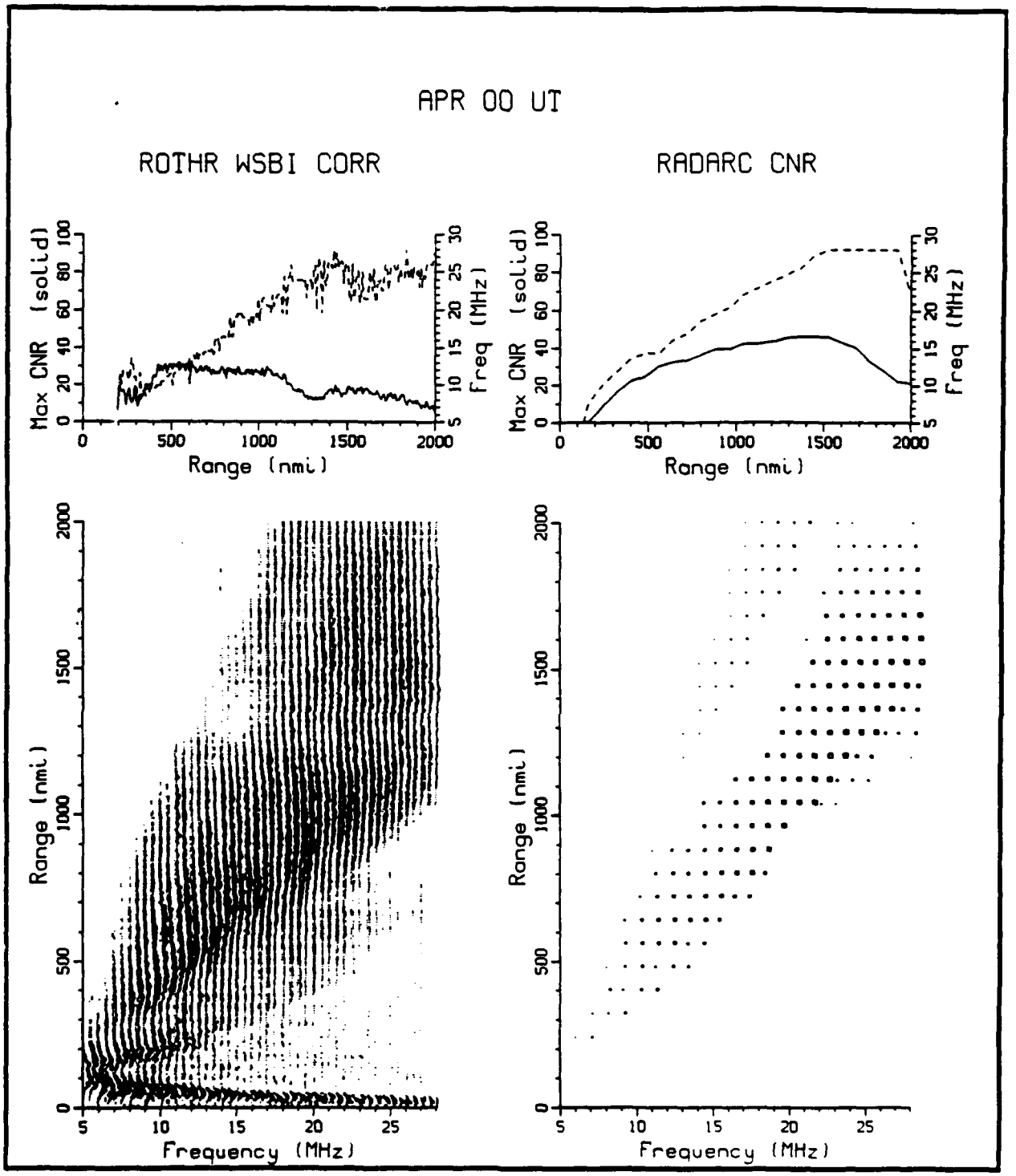

Figure 4.3. ROTHR widesweep backscatter ionogram (WSBI) vs. RADARC clutter-to-noise (CNR) map for 0 UT (noon in Amchitka) of April.

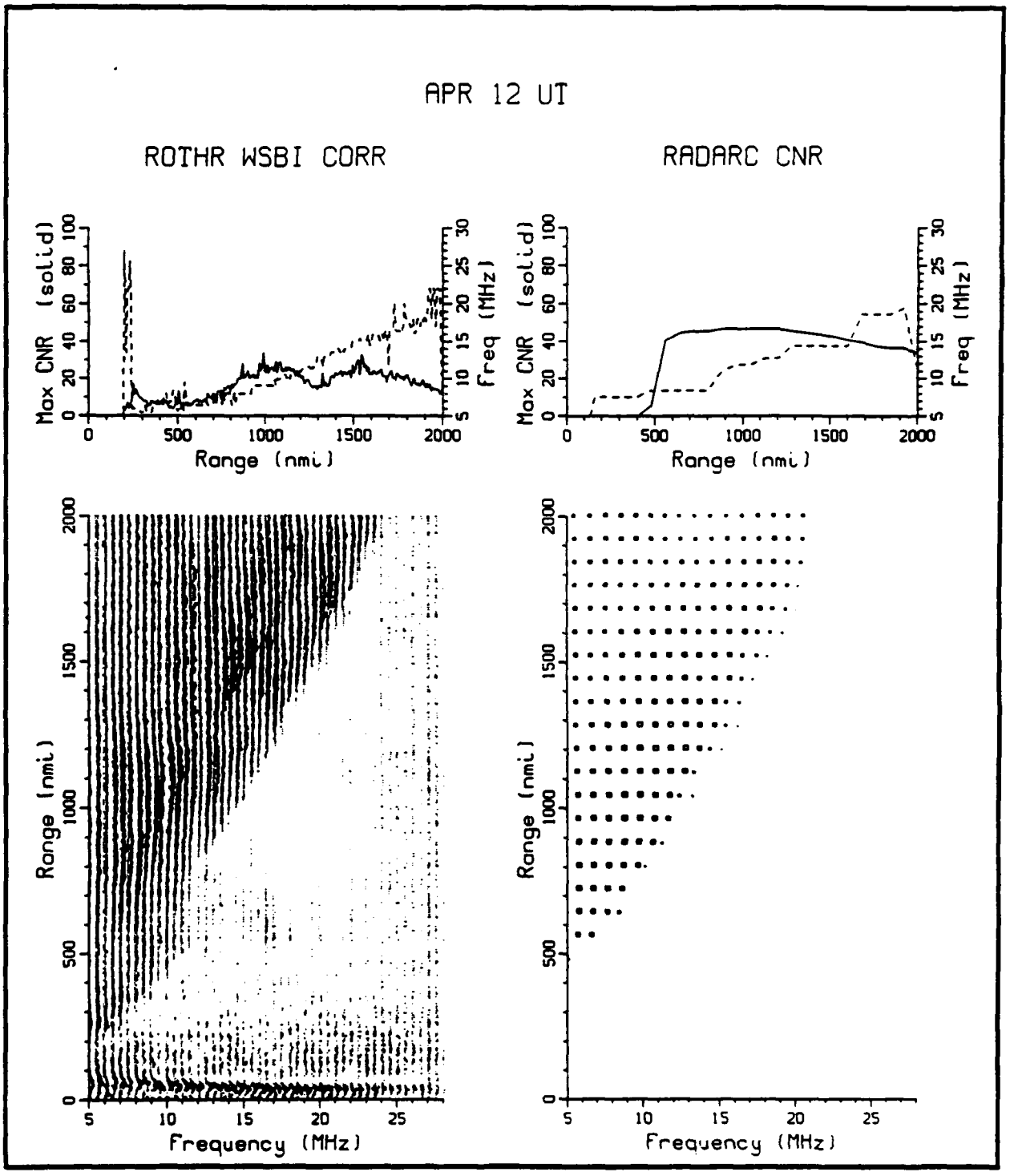

Figure 4.4. ROTHR widesweep backscatter ionogram (WSBI) vs. RADARC clutter-to-noise (CNR) map for 12 UT (midnight in Amchitka) of April.

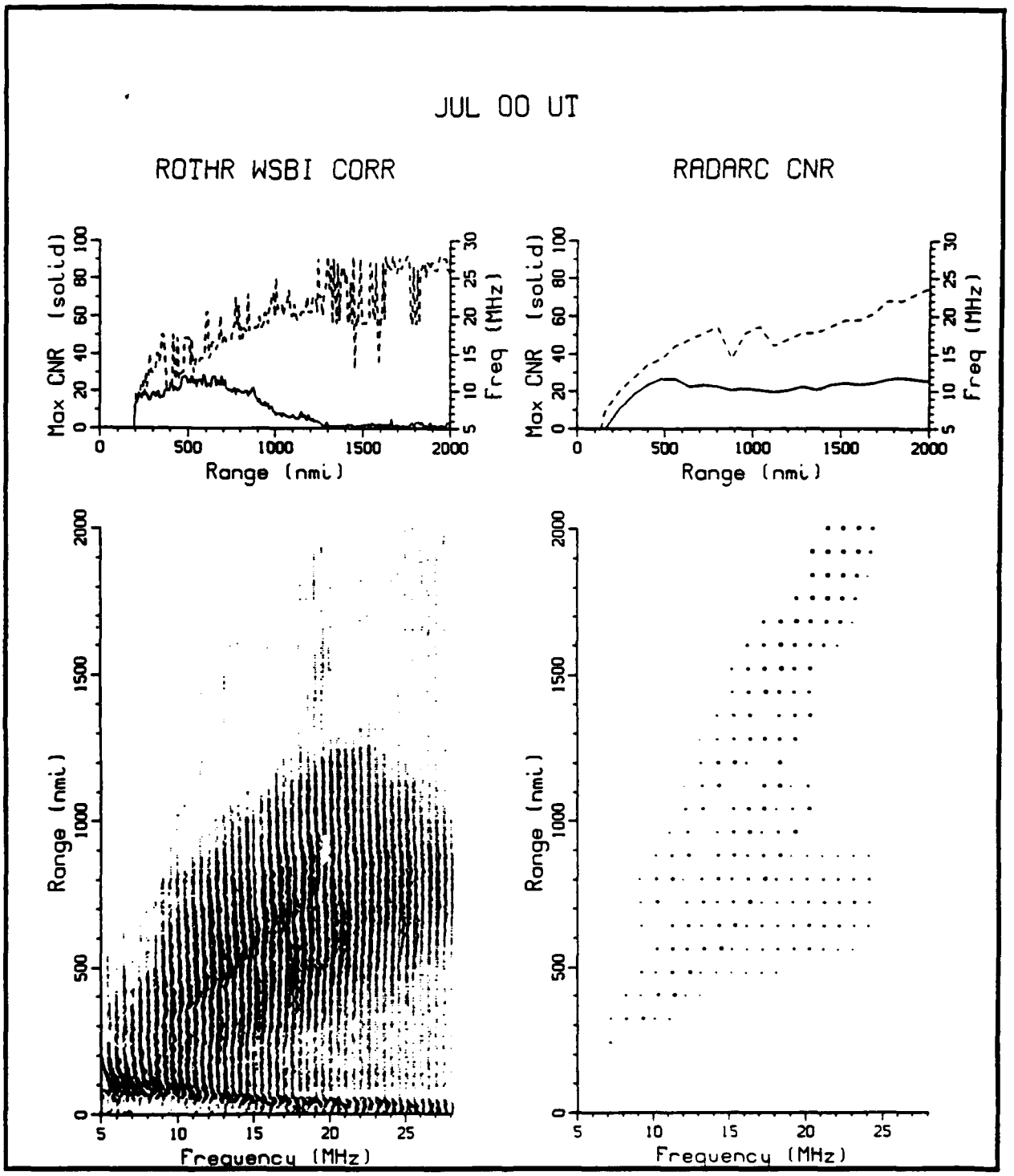

Figure 4.5. ROTHR widesweep backscatter ionogram (WSBI) vs. RADARC clutter-to-noise (CNR) map for 0 UT (noon in Amchitka) of July.

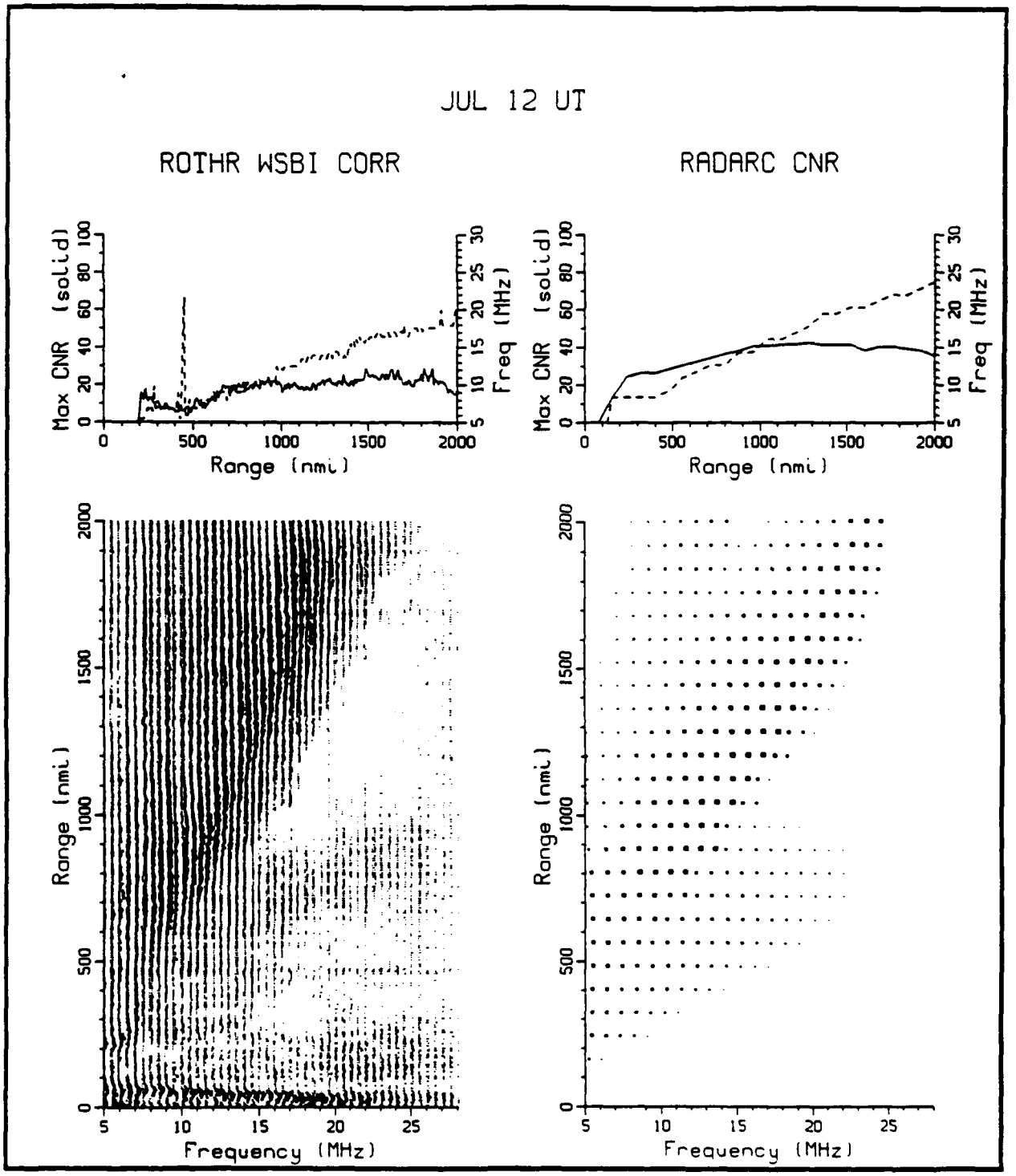

Figure 4.6. ROTHR widesweep backscatter ionogram (WSBI) vs. RADARC clutter-to-noise (CNR) map for 12 UT (midnight in Amchitka) of July.

Appendix C

Comparison of RADARC Predicted Clutter and Noise and ROTHR Data from Amchitka

Figures 5.1 to 6.6

The following plots compare RADARC predictions with measured data from Amchitka. The data consists of peaks (clutter maximum near 0 Hz) and noise (average in dB of power at + and - WRF/4). The latest version (2.0) of RADARC is shown.

Data is shown for hours 00 UT (noon in Amchitka) and 12 UT (midnight in Amchitka) for January, April, and July of 1991. All plots are restricted to an angular sector of 0 to 10 degrees with respect to boresight, so that the geography (and hence reflection) at a given range is relatively constant over azimuth. This geography consists of mixed land and sea from 500 to 1500 nm and mostly land from 1500 to 2000nm.

The data has been scaled in dBW to approximate the absolute level of power at the output of the array. The data has been smoothed by taking the median over all sixteen beams and over 100 nm range intervals.

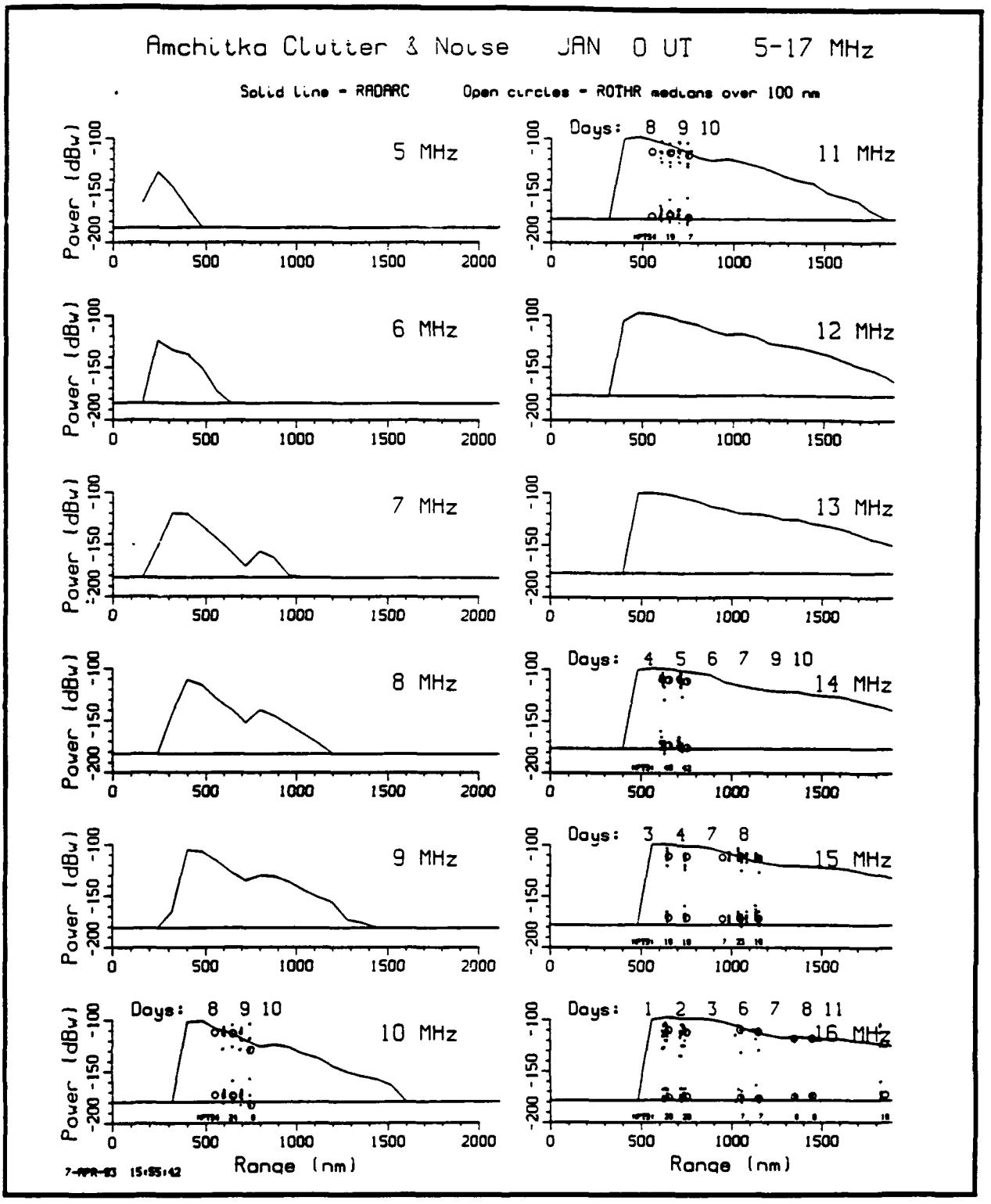

Figure 5.1. Radar backscatter power vs. range. Dots are ROTHR data points (peaks and noise) from Amchitka. Circles are medians of data points over 100 nm intervals. Solid lines are RADARC predictions (version 2.0). Data is for January 1991, 0 UT (local daytime), 5-17 MHz, 0 to 10 degrees with respect to boresight. Each subplot is a 1 MHZ band.

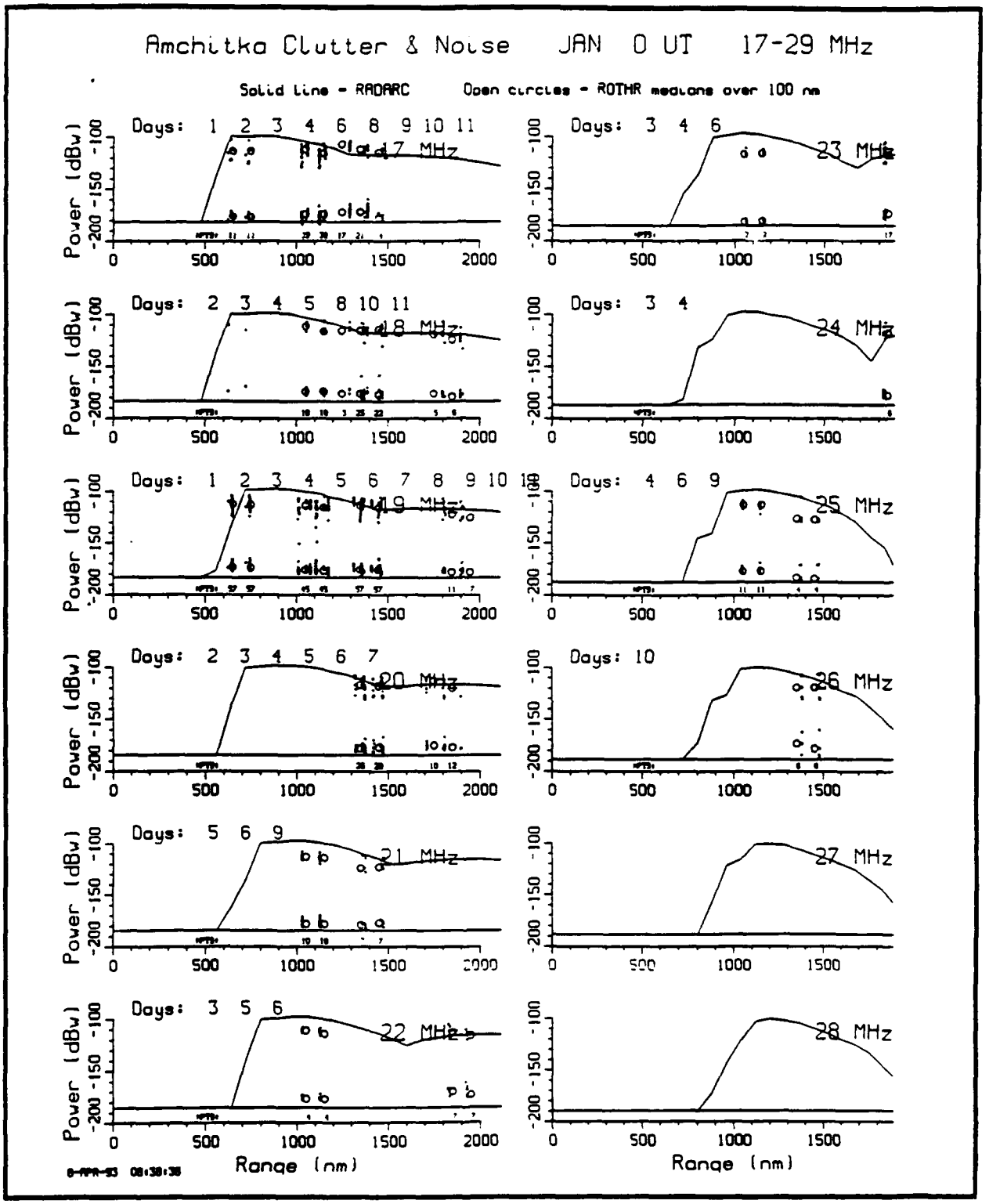

Figure 5.2. Radar backscatter power vs. range. Dots are ROTHR data points (peaks and noise) from Amchitka. Circles are medians of data points over 100 nm intervals. Solid lines are RADARC predictions (version 2.0). Data is for January 1991, 0 UT (local daytime), 17-28 MHz, 0 to 10 degrees with respect to boresight. Each subplot is a 1 MHZ band.

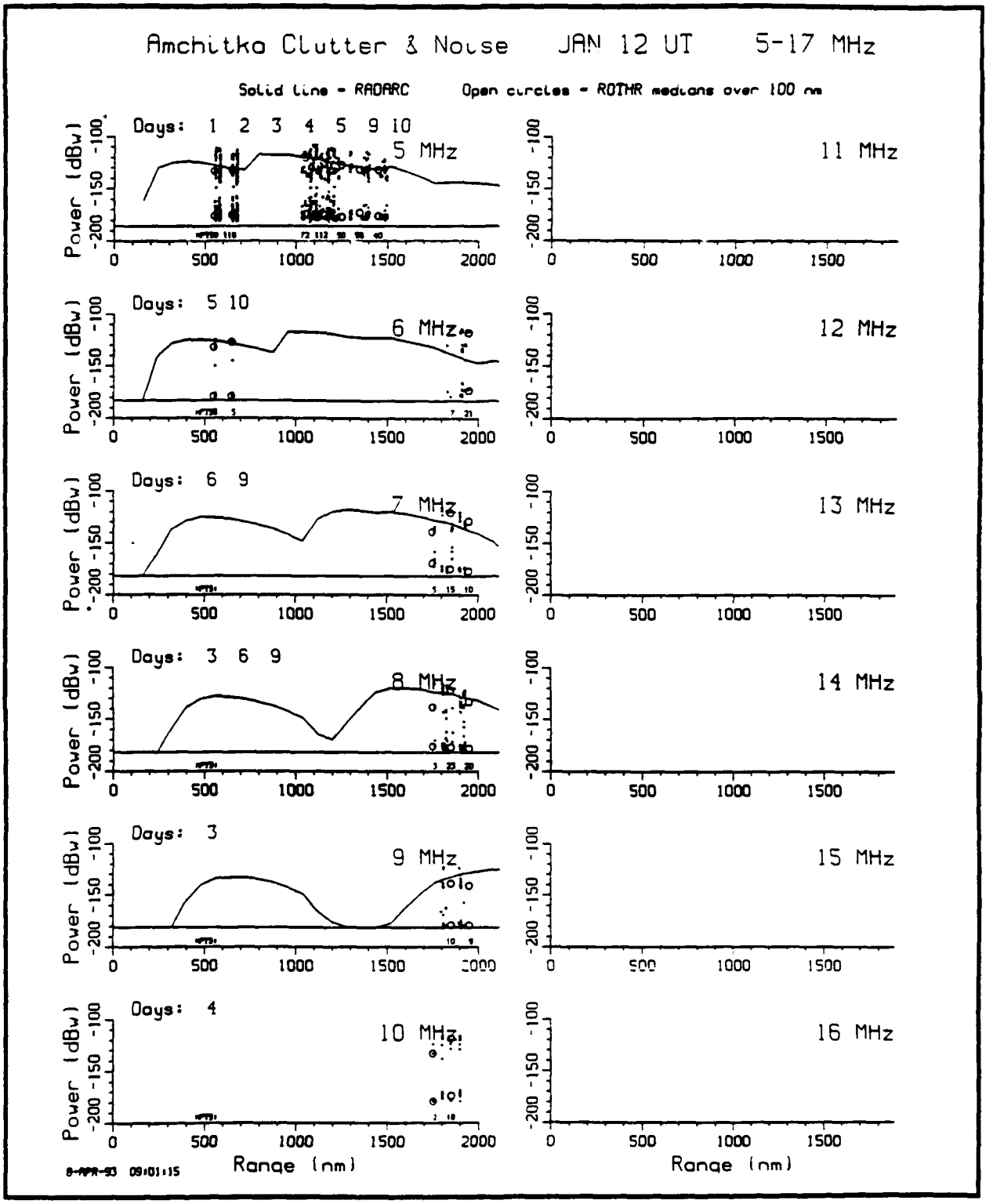

Figure 5.3. Radar backscatter power vs. range. Dots are ROTHR data points (peaks and noise) from Amchitka. Circles are medians of data points over 100 nm intervals. Solid lines are RADARC predictions (version 2.0). Data is for January 1991, 12 UT (local nighttime), 5-17 MHz, 0 to 10 degrees with respect to boresight. Each subplot is a 1 MHZ band.

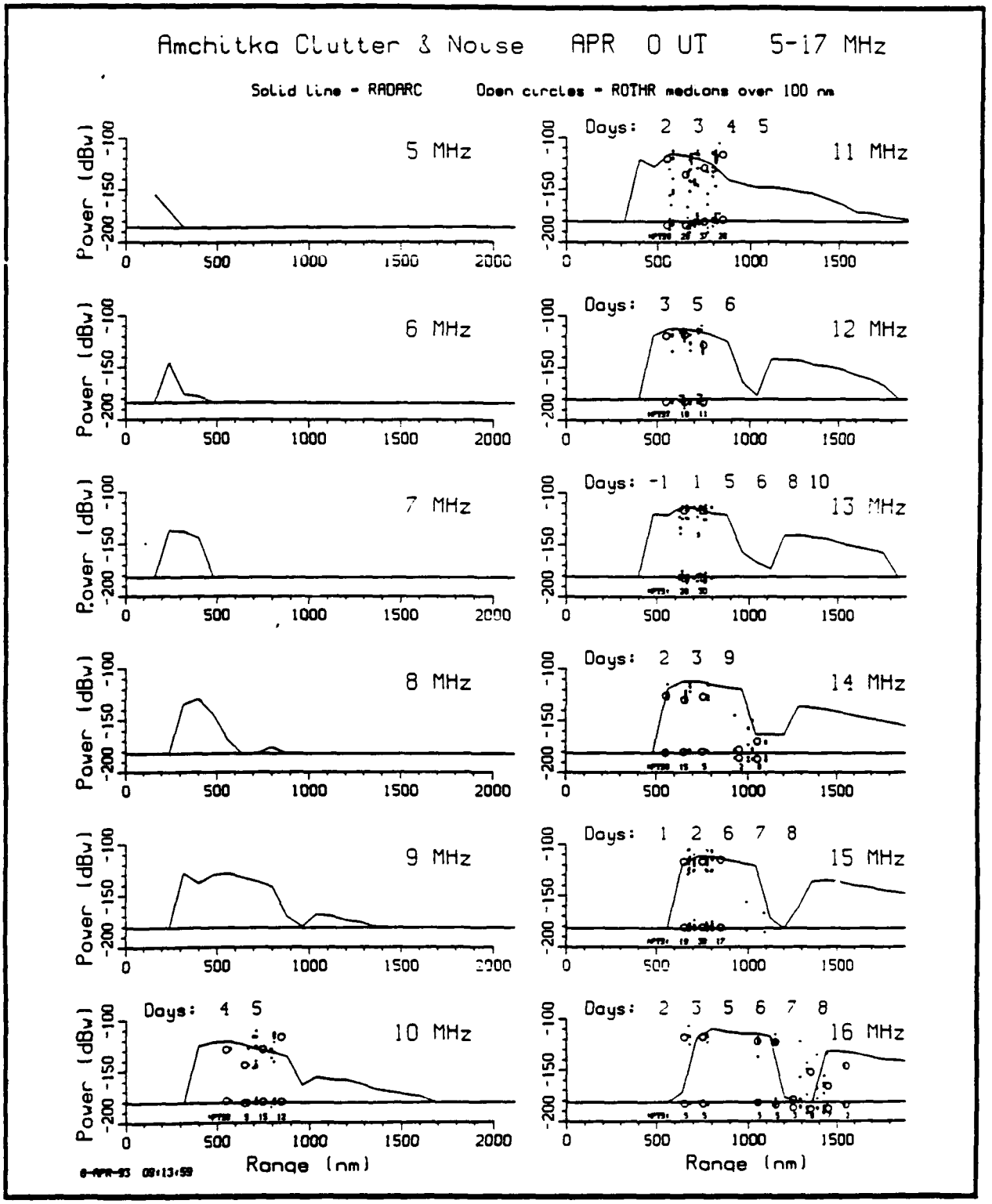

Figure 5.4. Radar backscatter power vs. range. Dots are ROTHR data points (peaks and noise) from Amchitka. Circles are medians of data points over 100 nm intervals. Solid lines are RADARC predictions (version 2.0). Data is for April 1991, 0 UT (local daytime), 5-17 MHz, 0 to 10 degrees with respect to boresight. Each subplot is a 1 MHZ band.

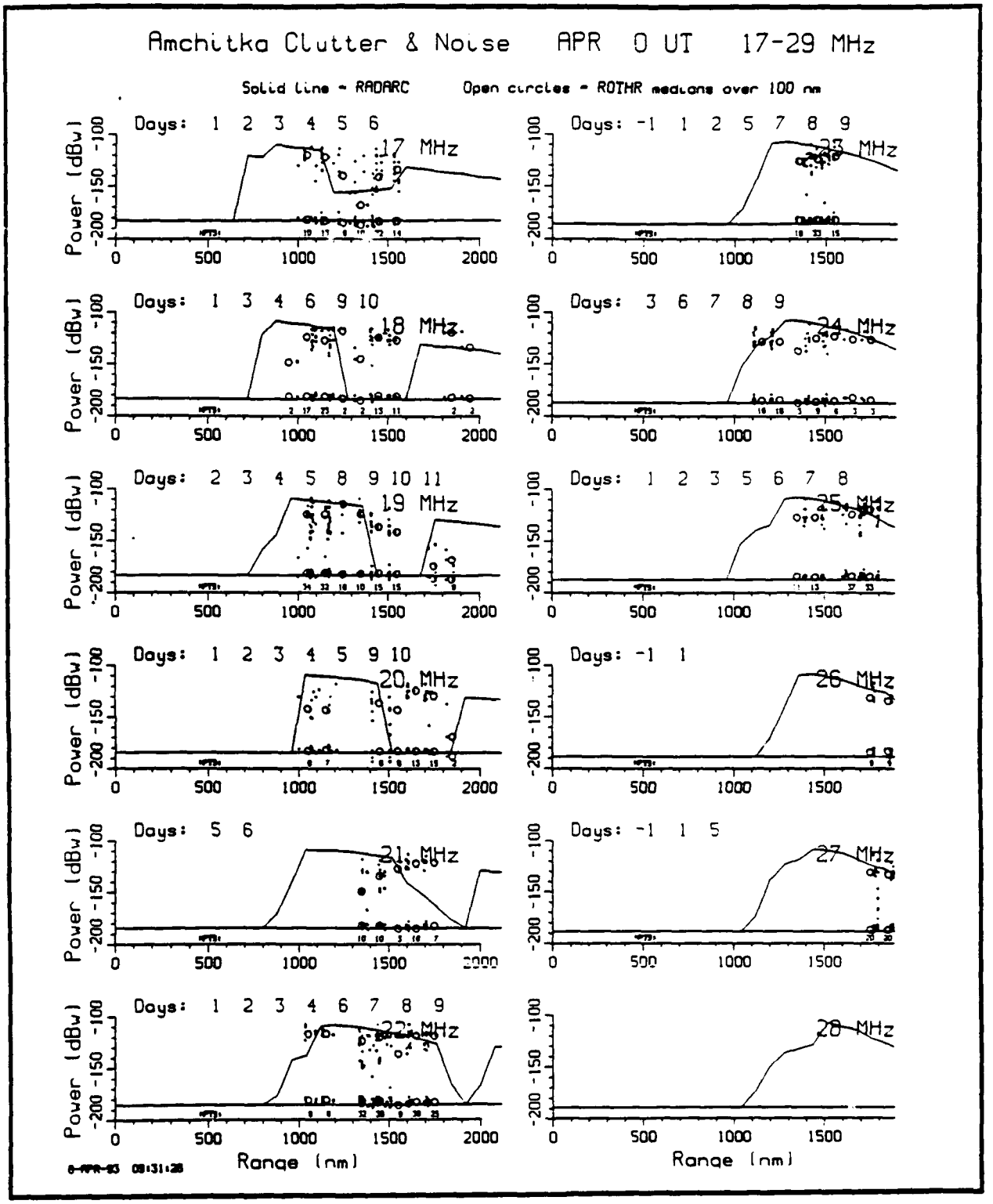

Figure 5.5. Radar backscatter power vs. range. Dots are ROTHR data points (peaks and noise) from Amchitka. Circles are medians of data points over 100 nm intervals. Solid lines are RADARC predictions (version 2.0). Data is for April 1991, 0 UT (local daytime), 17- 28 MHz, 0 to 10 degrees with respect to boresight. Each suɹplot is a 1 MHZ band.

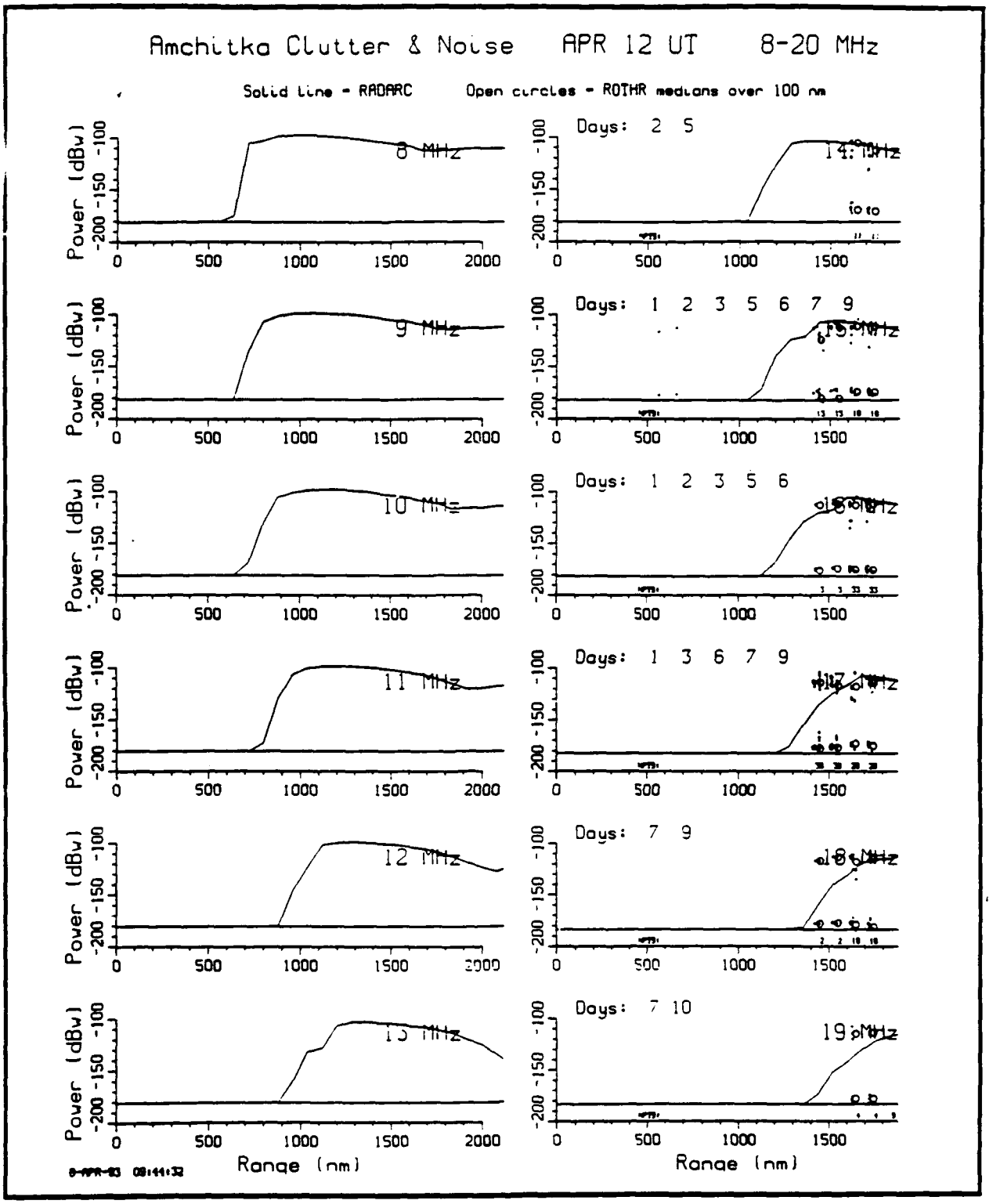

Figure 5.6. Radar backscatter power vs. range. Dots are ROTHR data points (peaks and noise) from Amchitka. Circles are medians of data points over 100 nm intervals. Solid lines are RADARC predictions (version 2.0). Data is for April 1991, 12 UT (local nighttime), 8-20 MHz, 0 to 10 degrees with respect to boresight. Each subplot is a 1 MHZ band.

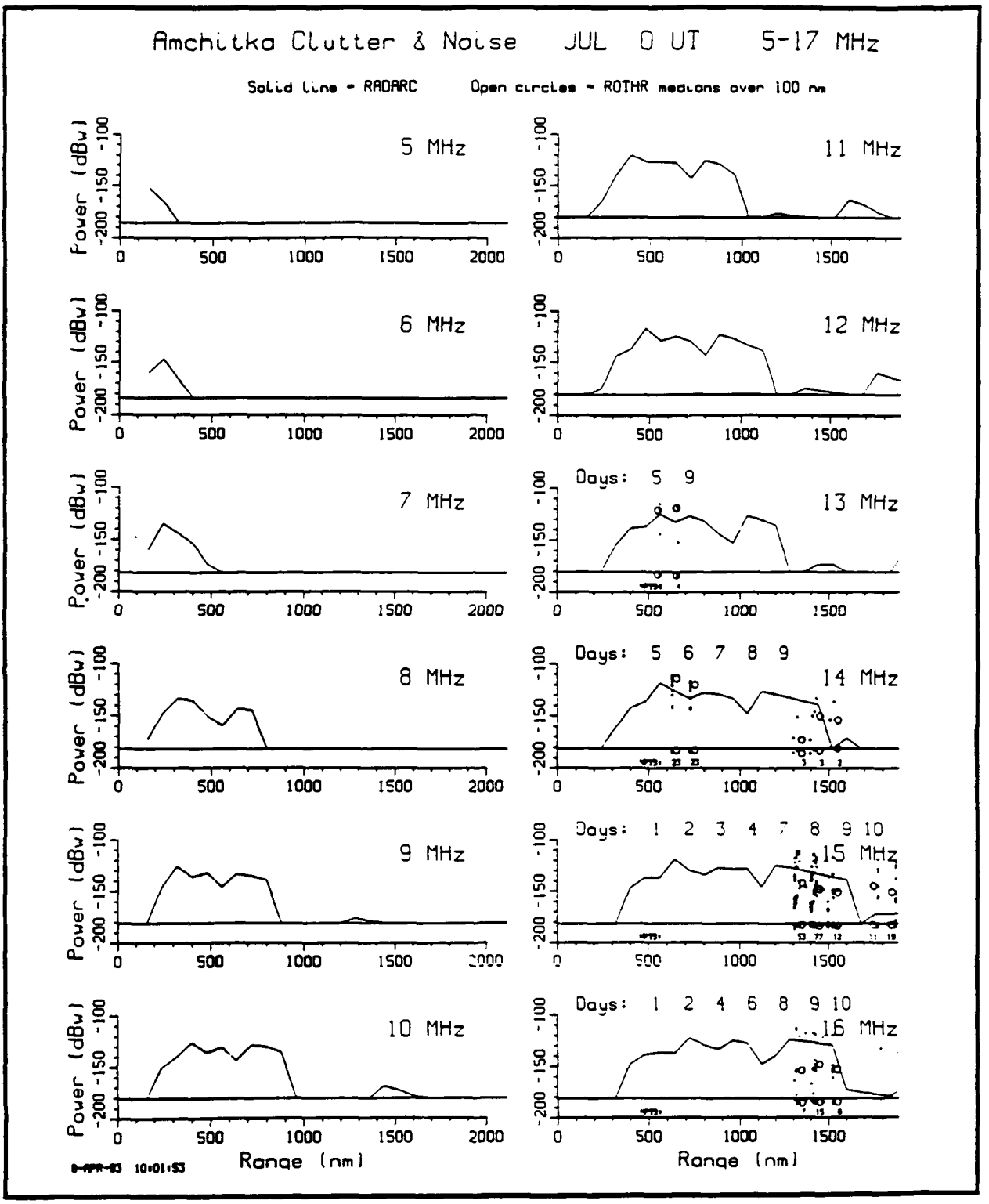

Figure 5.7. Radar backscatter power vs. range. Dots are ROTHR data points (peaks and noise) from Amchitka. Circles are medians of data points over 100 nm intervals. Solid lines are RADARC predictions (version 2.0). Data is for July 1991, 0 UT (local daytime), 5-17 MHz, 0 to 10 degrees with respect to boresight. Each subplot is a 1 MHZ band.

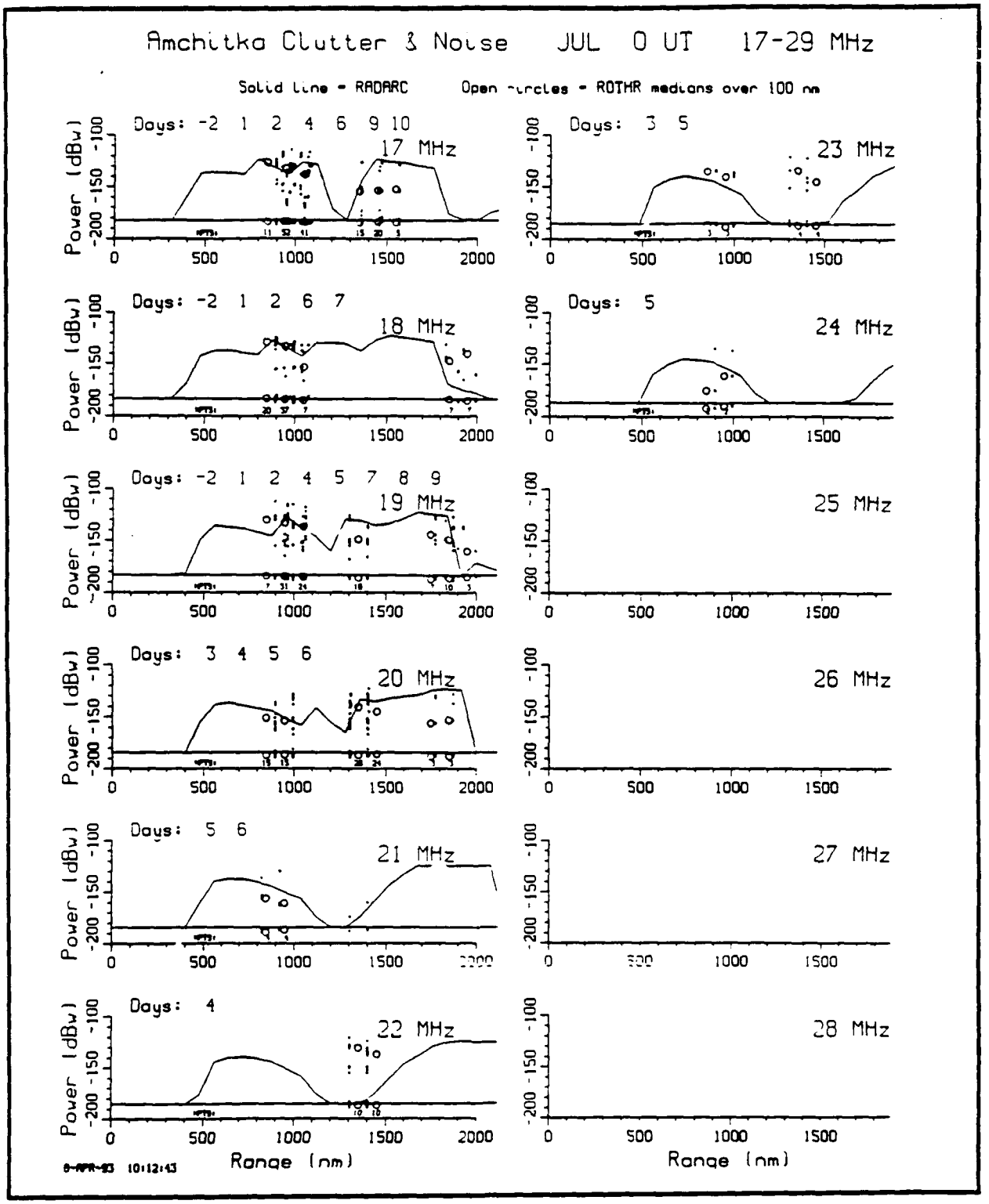

Figure 5.8. Radar backscatter power vs. range. Dots are ROTHR data points (peaks and noise) from Amchitka. Circles are medians of data points over 100 nm intervals. Solid lines are RADARC predictions (version 2.0). Data is for July 1991, 0 UT (local daytime), 17-28 MHz, 0 to 10 degrees with respect to boresight. Each subplot is a 1 MHZ band.

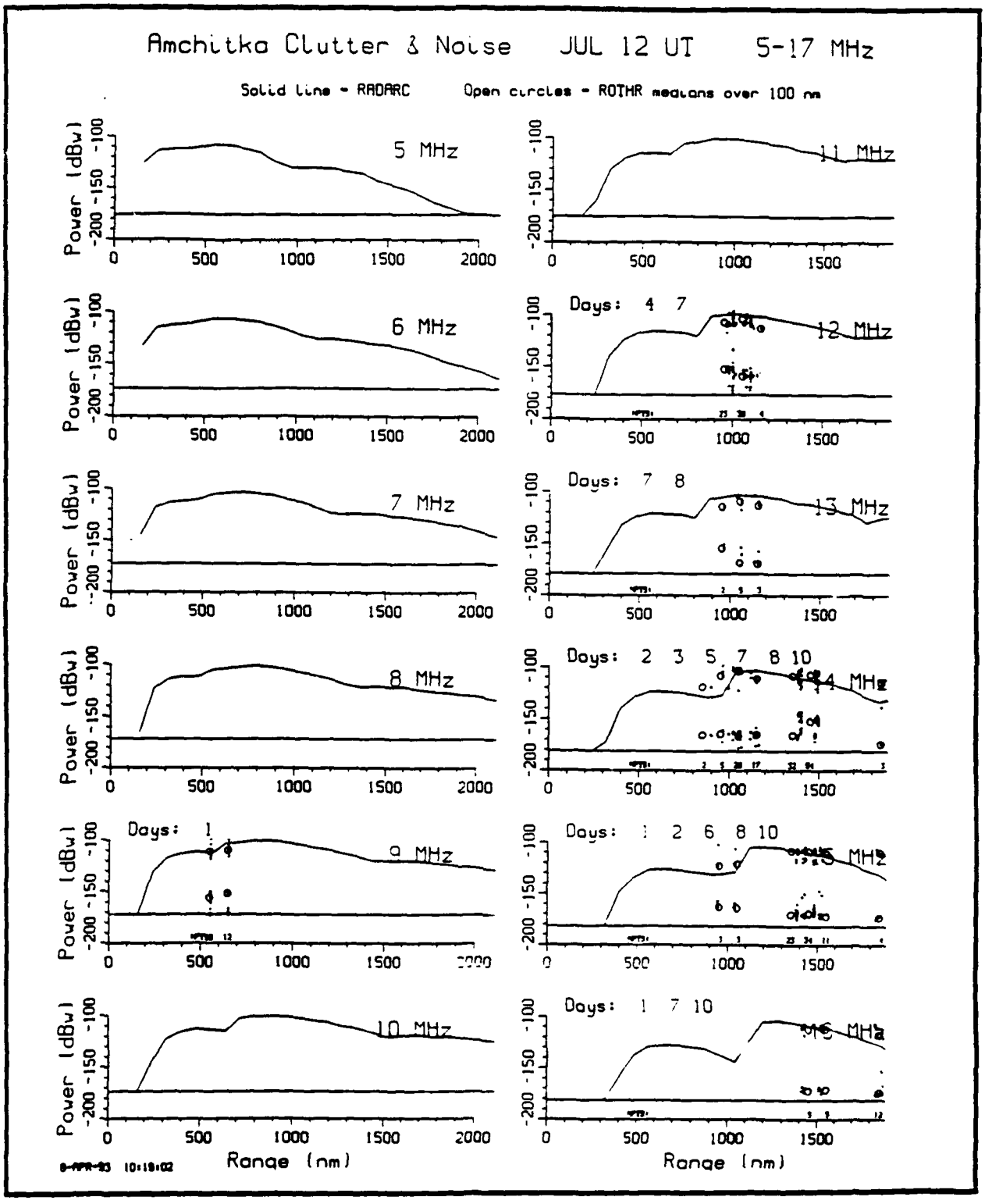

Figure 5.9. Radar backscatter power vs. range. Dots are ROTHR data points (peaks and noise) from Amchitka. Circles are medians of data points over 100 nm intervals. Solid lines are RADARC predictions (version 2.0). Data is for July 1991, 12 UT (local nighttime), 5-17 MHz, 0 to 10 degrees with respect to boresight. Each subplot is a 1 MHZ band.

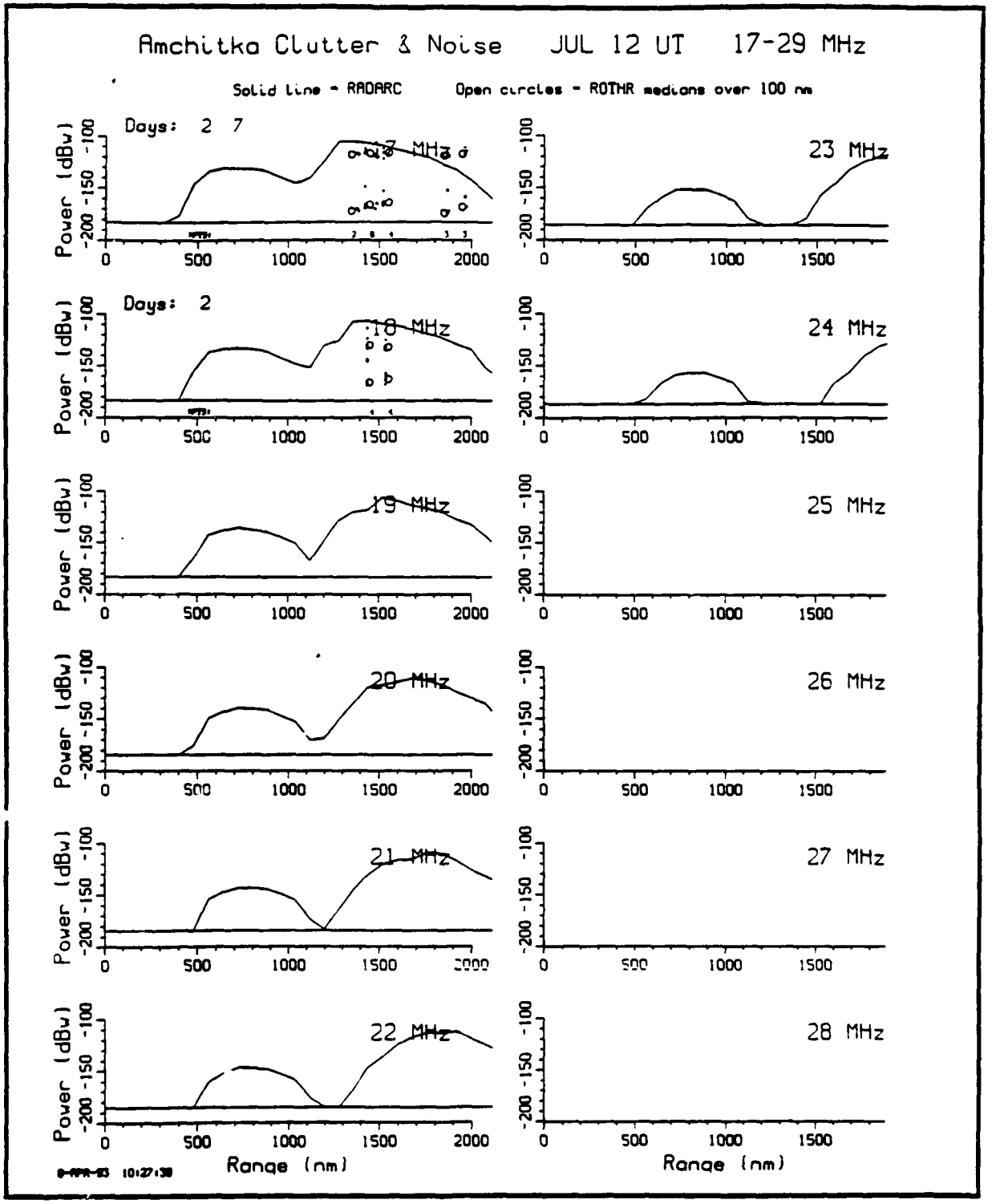

Figure 5.10. Radar backscatter power vs. range. Dots are ROTHR data points (peaks and noise) from Amchitka. Circles are medians of data points over 100 nm intervals. Solid lines are RADARC predictions (version 2.0). Data is for July 1991, 12 UT (local nighttime), 17-28 MHz, 0 to 10 degrees with respect to boresight. Each subplot is a 1 MHZ band.

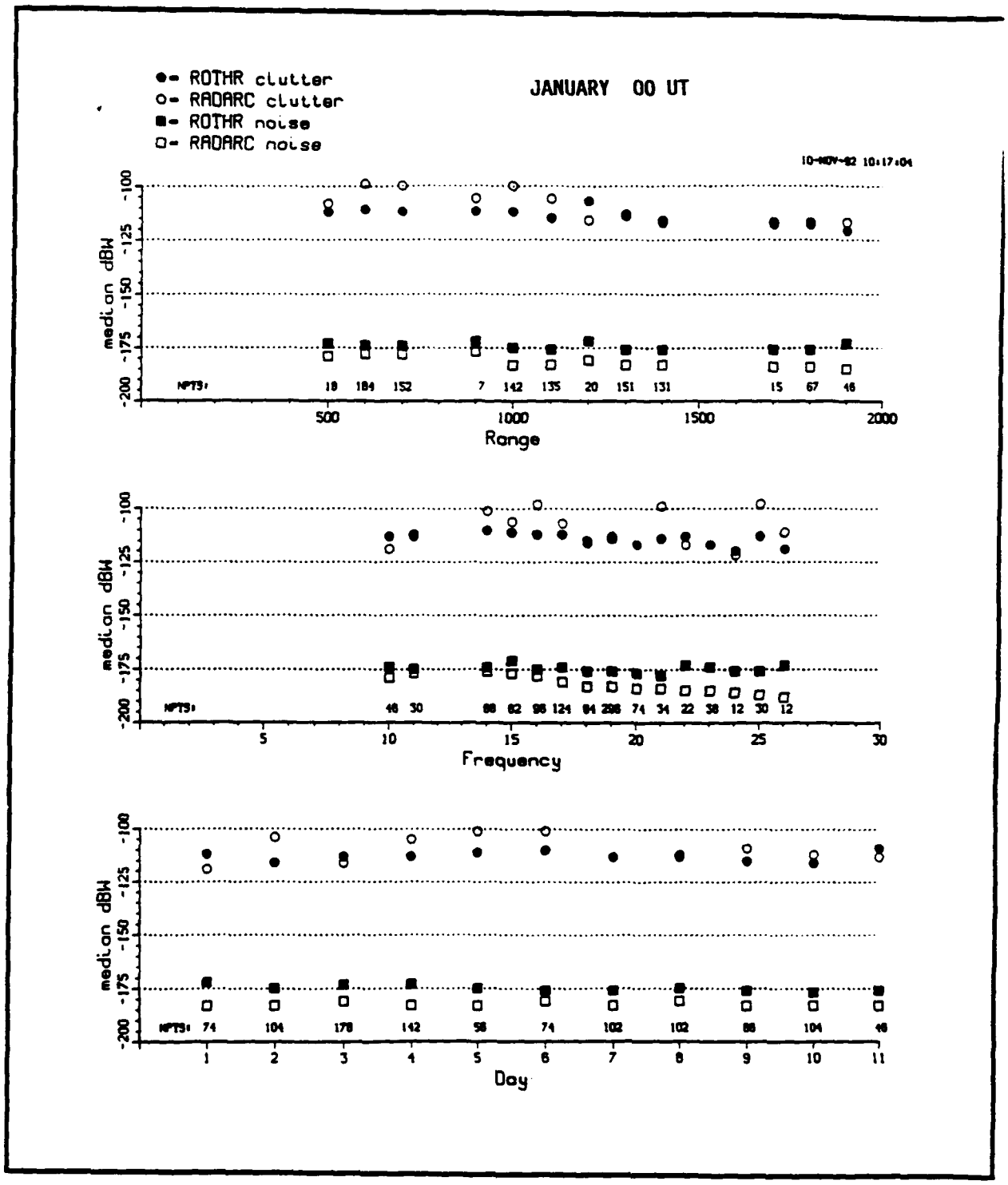

Figure 6.1 . Radar backscatter power medians with respect to range, frequency, and day for 00 UT of January. The data points are the same as in the corresponding month and hour of the preceding set of figures. For example, the median over range at 500 nm includes all data points between 500 and 600 nm, regardless of day or frequency. The number of data points in the median is shown along the bottom.

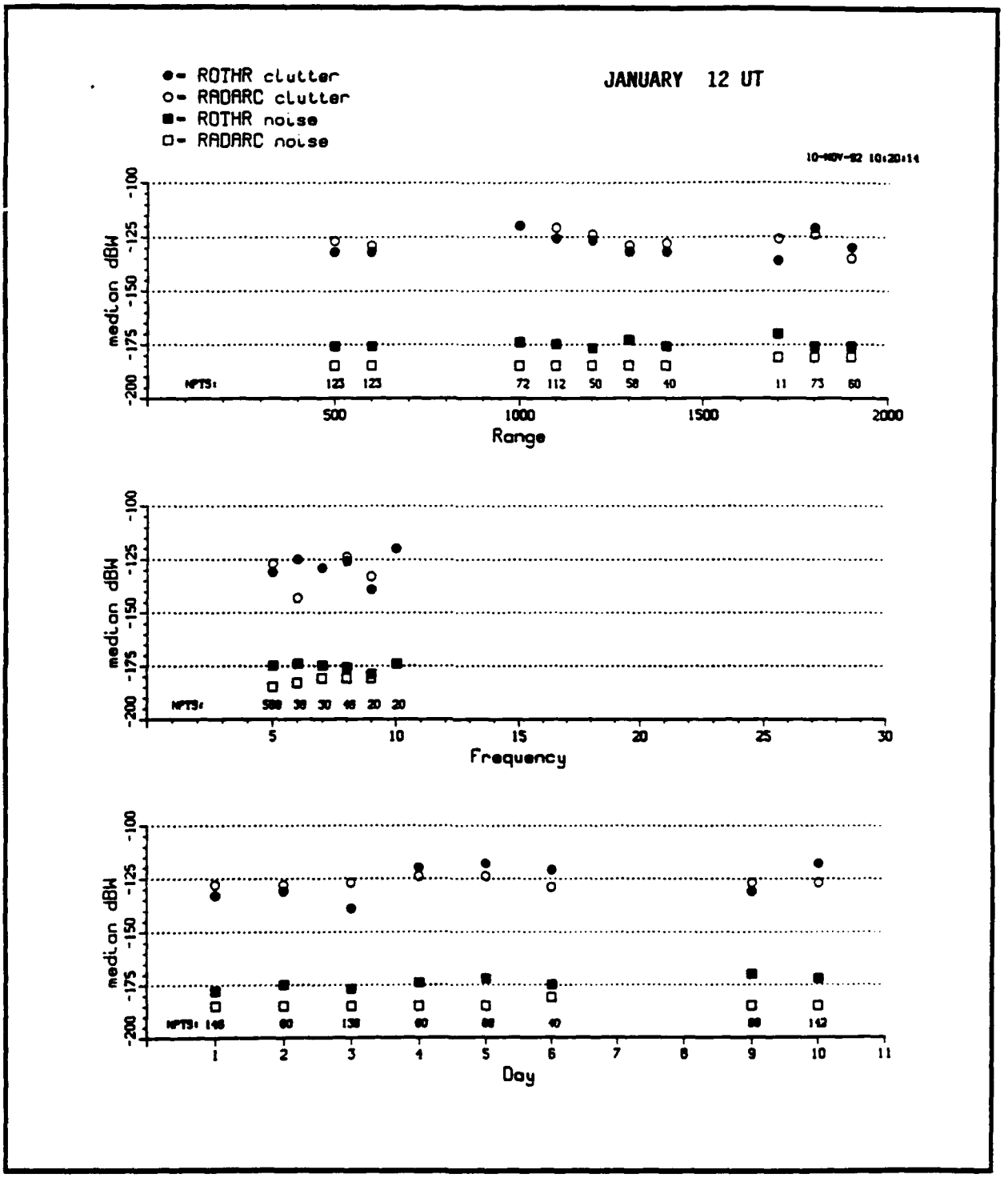

Figure 6.2. Radar backscatter power medians with respect to range, frequency, and day for 12 UT of January. The data points are the same as in the corresponding month and hour of the preceding set of figures. For example, the median over range at 500 nm includes all data points between 500 and 600 nm, regardless of day or frequency. The number of data points in the median is shown along the bottom.

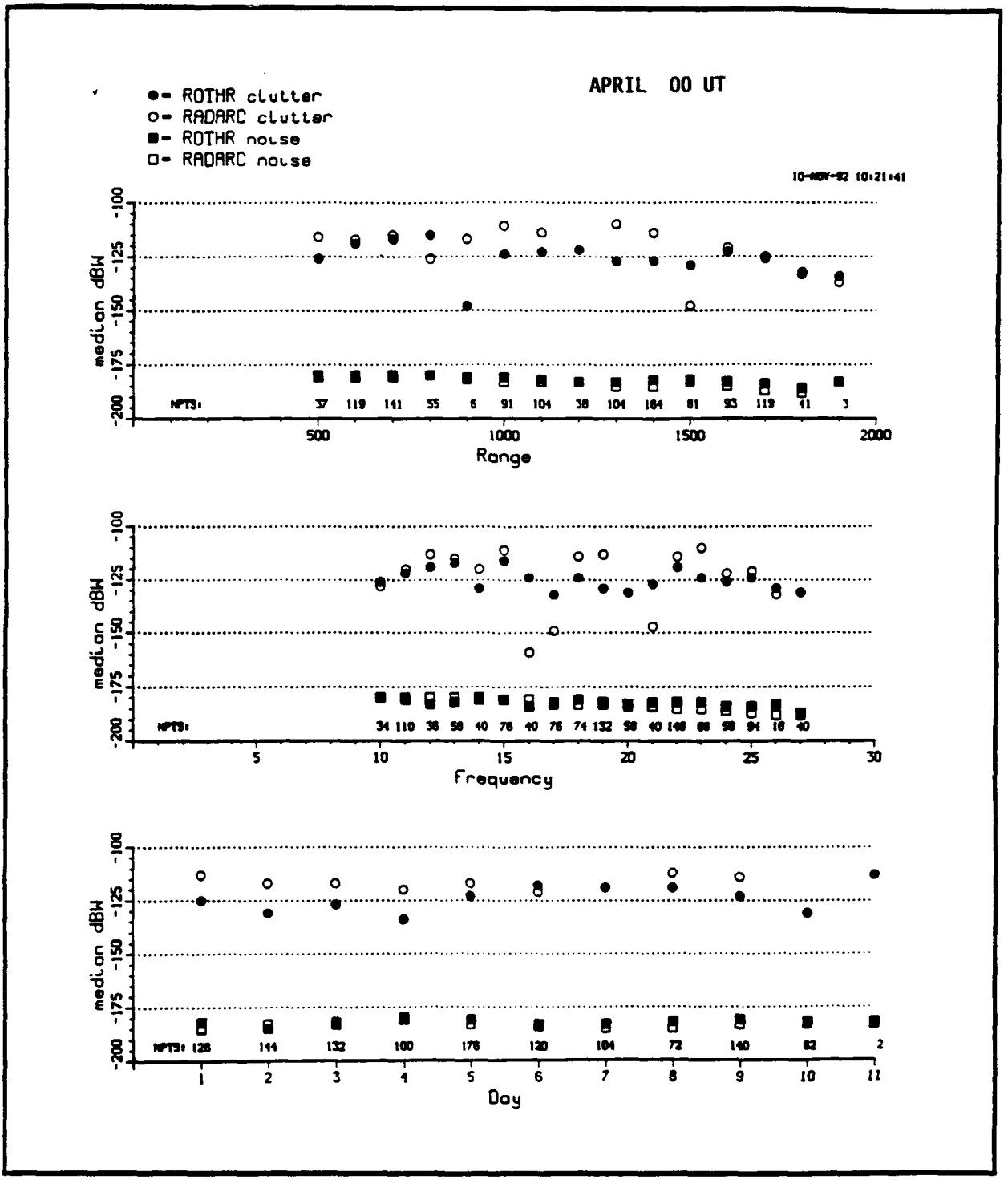

Figure 6.3. Radar backscatter power medians with respect to range, frequency, and day for 00 UT of April. The data points are the same as in the corresponding month and hour of the preceding set of figures. For example, the median over range at 500 nm includes all data points between 500 and 600 nm, regardless of day or frequency. The number of data points in the median is shown along the bottom.

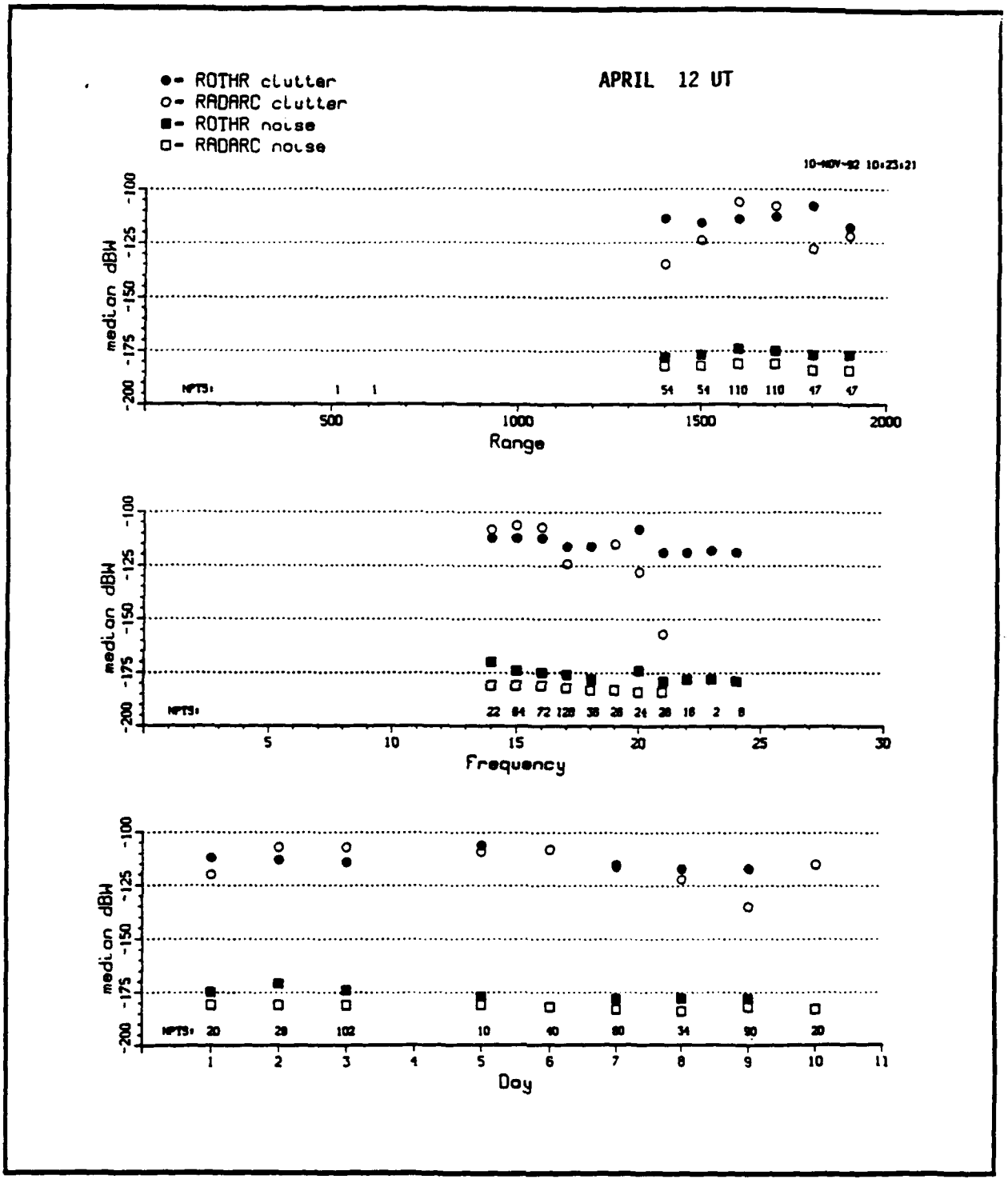

Figure 6.4. Radar backscatter power medians with respect to range, frequency, and day for 12 UT of April. The data points are the same as in the corresponding month and hour of the preceding set of figures. For example, the median over range at 500 nm includes all data points between 500 and 600 nm, regardless of day or frequency. The number of data points in the median is shown along the bottom.

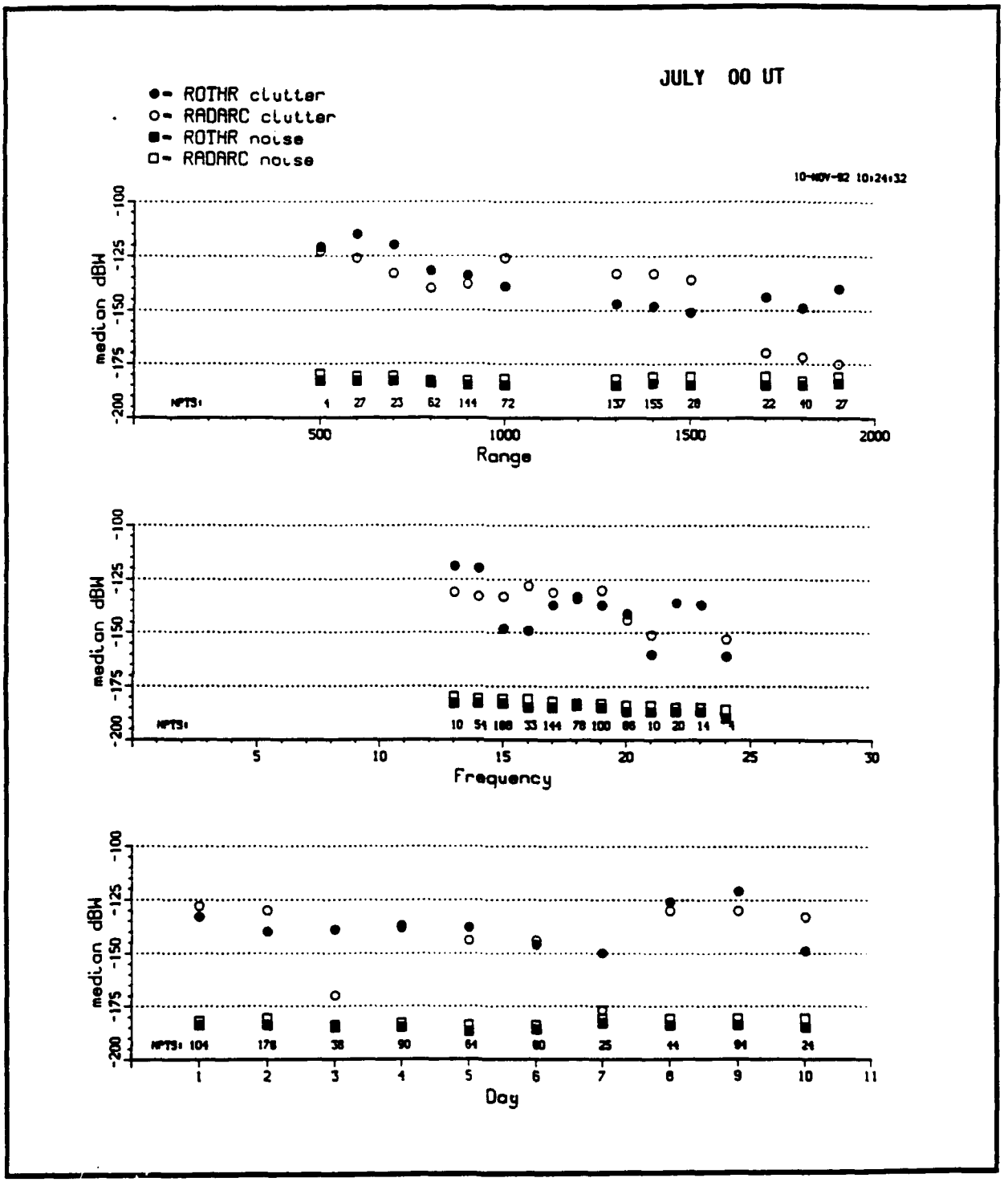

Figure 6.5 Radar backscatter power medians with respect to range, frequency, and day for 00 UT of July. The data points are the same as in the corresponding month and hour of the preceding set of figures. For example, the median over range at 500 nm includes all data points between 500 and 600 nm, regardless of day or frequency. The number of data points in the median is shown along the bottom.

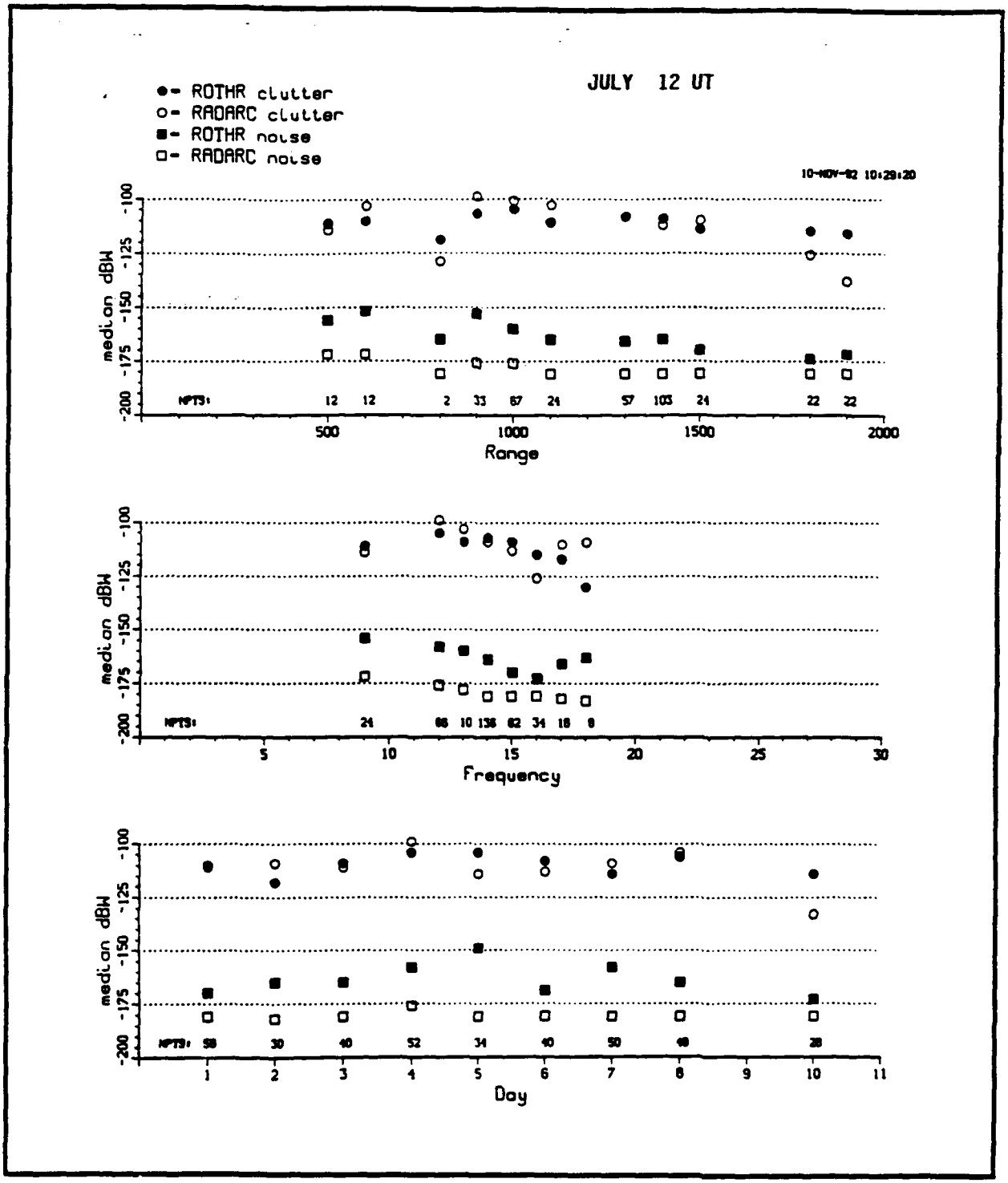

Figure 6.6. Radar backscatter power medians with respect to range, frequency, and day for 12 UT of July. The data points are the same as in the corresponding month and hour of the preceding set of figures. For example, the median over range at 500 nm includes all data points between 500 and 600 nm, regardless of day or frequency. The number of data points in the median is shown along the bottom.